1-1-2019

Atomic-Local Environments of Single-Atom Catalysts: Synthesis, Electronic Structure, and Activity

Weihong Lai
University of Wollongong, Xijing University, weihongl@uow.edu.au

Zongcheng Miao
Xijing University

Yunxiao Wang
University of Wollongong, yunxiao@uow.edu.au

Jiazhao Wang
University of Wollongong, jiazhao@uow.edu.au

Shulei Chou
University of Wollongong, shulei@uow.edu.au

Atomic-Local Environments of Single-Atom Catalysts: Synthesis, Electronic Structure, and Activity

Abstract

Single-atom catalysts (SACs) hold great promise for maximizing atomic efficiency of supported metals via the ultimate utilization of every single atom. The foreign isolated substitutions anchored on different supports build varieties of local structural centers, changing the physical and chemical properties. Thus, distinct atomic local environments for single-atom catalysts are essential for determining superior catalytic performance for a wide variety of chemical reactions. The examples of synthesizing single atoms on various supports presented here deepen the understanding of the different structural and electronic properties of SACs, in which the metal single atom does not bind with any other atoms of this metal, but substantially interacts with the support ions. Due to the strong support effects, the ubiquitous aggregation of metal single atoms can be addressed, achieving highly stable SACs. This review discusses recent progress in theoretical electronic effects between atomic dopants and supports, which reveal the electronic structures of various SACs and offers guidance for rational prediction and design of highly stable and reactive SACs. It is argued that tuning this interaction by the selection of the supports toward favorable atomic and electronic structures on the surface should be taken into consideration for the development of more efficient SACs.

Disciplines

Engineering | Physical Sciences and Mathematics

Publication Details

Lai, W., Miao, Z., Wang, Y., Wang, J. & Chou, S. (2019). Atomic-Local Environments of Single-Atom Catalysts: Synthesis, Electronic Structure, and Activity. Advanced Energy Materials, 9 (43), 1900722-1-1900722-30.

WILEY-VCH

DOI: 10.1002/ ((please add manuscript number))

Article type: (**Review**)

Atomic-local environments of single-atom catalysts: synthesis, electronic structure, and activity

Wei-Hong Lai, Zongcheng Miao, Yun-Xiao Wang*, Jia-Zhao Wang, Shu-Lei Chou**

W.H. Lai, Prof. Z.C. Miao

Key laboratory of Organic Polymer Photoelectric Materials, School of Science, Xijing University, Xi'an, 710123, Shaanxi, People's Republic of China

*E-mail: miaozongcheng@xijing.edu.cn

W.H. Lai, Dr. Y. X. Wang, Prof. J.Z. Wang, Prof. S. L. Chou

Institute for Superconducting and Electronic Materials, Australian Institute of Innovative Materials, University of Wollongong, Innovation Campus, Squires Way, North Wollongong, New South Wales 2500, Australia

E-mail: yunxiao@uow.edu.au; shulei@uow.edu.au

Abstract:

Single-atom catalysts (SACs) hold great promise for maximizing atomic efficiency of supported metals by achieving the ultimate utilization of every single atom. The foreign isolated substitutions anchored on different supports build varieties of local structural centres, changing the physical orbital science, band gap, electronic density, and surface chemistry. Thus, distinct atomic local environments for single-atom catalysts are essential on determining superior catalytic performance for a wide variety of chemical reactions. The examples on synthesizing single atoms on various supports here deepen understanding on the different structural and electronic properties of SACs from those of clusters and nanoparticles, in which the metal single atom does not bind with any other atoms of this metal, but substantially interact with the support ions. Due to the strong support effects, the ubiquitous aggregation of metal

single atoms can be well addressed to achieve highly stable SACs. This review involves recent progress on theoretical electronic effects between atomic dopants and supports, which reveals the electronic structures of various SACs and offers a guidance for rational prediction and design of highly stable and reactive SACs. We believe that tuning the interaction by selection of the supports towards favourable atomic and electronic structures on the surface should be taken into consideration for the development of more efficient SACs.

Keywords: single atom catalysts; support effects; SACs synthesis; catalytic reactions; atomic-local environments

1. Introduction

In order to make use of alternative energy sources, including biomass, solar or nuclear for the future, it is imperative to explore favourable heterogeneous catalysts for fuel cells and photovoltaic cells.[1] Supported metal catalysts are the most extensively used, which are typically consisted of metal components finely dispersed/coordinated/stabilized on a variety of host matrices. Since the size of metal components plays a pivotal role in determining the reactivity and selectivity of the heterogeneous catalysts, enormous efforts are invested in downsizing the metal particles to atomic level for ultimate catalysis over last decade. Therefore, single-atom catalysts (SACs), integrating isolated metal atoms on appropriate supports, become a new frontier in heterogeneous catalysts towards material synthesis and potential applications towards diverse catalytic reactions.[2] The ultimate low-coordination environment of single atoms (SAs) could achieve maximum metal dispersion to expose every atom as catalytically active sites. Meanwhile, the intrinsic quantum size effects with electrons confinement are responsible for discrete energy level distributions and distinctive the highest occupied molecular orbital - lowest occupied molecular orbital (HOMO-LUMO) gaps.[3] Beyond that, SACs usually exhibit distinct electronic structures based on their unique atomic-local environments, thus are expected to deliver extraordinary catalytic performance.

The design and fabrication of SACs has been focused on stabilizing metal SAs against sintering/leaching and achieving high loading ratio. Recently, it is found that the choice of supports plays critical roles, which not only acts as physical carriers to support the SAs but also significantly influences on the electronic configurations of the metal SAs, thus catalytically or chemically impact on the catalytic properties of SACs. A concept of strong metal-support interaction (SMSI) was brought out in heterogeneous catalysis field in 1980s,[4] which is employed to understand the large electronic perturbations for the supported metals due to contact with the supports. Also, this SMSI effect was extended into SACs, which was believed to alter the charge state of the SAs metal by electron transfer between SAs and a support, leading to the activated reactants and enhanced catalytic properties of the SAs.[5] It is interesting that SACs possess extremely radical local-atomic environments with the absence of metallic binding but the strongest metal-support interaction. The understanding on atomic-local environments of single atoms is essential but still very ambiguous.

The developments on both atomic-resolution characterization techniques and theoretical modelling are unveiling the mysteries of SACs. Over decades, research community has devoted to find effective approaches to strongly anchor the metal SAs to form highly stable and reactive catalytic active centres for desired catalytic reactions; yet, it remains a grand challenge to guide the prediction and design of highly stable and reactive SACs under realistic conditions. Some reviews on SACs have been published in recent years,[6] to the best of our knowledge, none of them emphasizes on the tunable atomic-local environments of SACs, which are determined by the selection of supports and lead to adjustable electronic configurations of SAs, thereby achieving more efficient SACs as regards of catalytic activity, stability, and selectivity. In this context, this review will involve the significant progress on the synthesis of novel SACs on various anchoring sites of supports. We will then primarily focus on understanding the selection of supports for the synthesis of SACs with high thermal stability. Moreover, based

on different atomic-local environments, electronic structures of SACs on different supports have been understood via theoretical calculations. The underlying mechanisms for various SACs fabrication and corresponding electrocatalytic applications are summarized, which lead to a better understanding of the role of single-atom species, supports selection, and SMSI effects for catalytic properties. Lastly, challenges and opportunities for future research on SACs will be present.

2. Support effects in synthesis of single atoms

2.1 Support effects for anchoring single atoms

The SACs are hardly stable since the surface energy is ultimately high due to the smallest particle size. The strong interaction between metal and support plays an essential role in creating stable and finely dispersed SACs and prevents them from aggregation. Three factors, including precursors, supports, and synthetic procedures, are extremely critical in controlling the interactions and optimizing the dispersion of isolated metal atoms. The commonly used supports and synthesis methods are listed in Table 1**,** which summarized corresponding effective catalytic reactions of the produced SACs as well. The essential prerequisite of SACs fabrication is to rationally select or modify supports with specific anchoring sites, which could stabilize single atoms under realistic reaction conditions with elevated temperatures and pressures. As illustrated in Figure 1, representative anchoring sites for single atoms with different atomic-local environments have been displayed, including low-index metal oxide facets, oxidic defects on metal oxides, nitrogen-doped sites, modified surface by organic ligands, and the surface of metal nanoclusters. Correspondingly, we displayed the commonly used supports and devoted to understanding the interaction between single atoms and these supports, which lays significant foundation for the design and synthesis of stable single-atom catalysts.

Table 1. A partial list of the supports and synthesis methods for producing supported SACs towards various catalytic reactions.

Support	SAs	Methods	Applications	Ref
CeO_2	Au_1 Pt_1	Coprecipitation-calcination; Atom trapping; Deposition-precipitation;	Preferential oxidation of CO (PROX); CO oxidation;	[7]
Al_2O_3	Pt_1 Au_1	Mass-selected soft-loading; Sol-gel calcination method; Impregnation-precipitation; Laser ablation;	CO oxidation; Hydrosilylation reactions; NO oxidation;	[8]
FeO_x	Ir_1 Au_1 Pt_1	Coprecipitation-calcination; Adsorption method Coprecipitation-calcination	Water gas shift (WGS) reaction; CO oxidation; Reduction of NO by H_2; Hydorogeneation of nitroarenes	[2, 9]
TiO_2	Pd_1 Pt_1	Impregnation-calcination	Styrene hydrogenation; CO oxidation;	[10]
ZnO	Pt_1 Au_1	Adsorption method	Methanol Steam Reforming	[11]
$ZnZrO_x$	Au_1	Impregnation-calcination	Ethanol dehydrogenation	[12]
MnO_2	Ag_1	Annealing method	HCHO oxidation	[13]
SiO_2	Pt_1	Impregnation-calcination	CO oxidation; WGS	[14]
VO_2	Rh_1	Adsorption method	Ammonia–borane hydrolysis	[15]
WO_x	Pt_1	Impregnation-calcination	Selective hydrogenolysis of glycerol	[16]
MoS_2	Pt_1 Ni_1 Co_1	Hydrothermal method; Hydrothermal method- calcination;	hydrogen evolution reaction (HER); Hydrodeoxygenation reaction (HDO)	[17]
TiN TiC	Pt_1	IWI method	Oxygen reduction reaction (ORR)	[18]
Graphene (G)	Pt_1 $Co_1 In_1$ Pd_1 Ni_1	Electron beam; Atomic layer deposition (ALD); Sputtering tool; Chemical exfoliation	Methanol oxidation reaction (MOR); Hydrogenation of 1,3-butadiene; HER;	[19]
Carbon	Nb_1 Au_1	Arc-discharge approach; Impregnation-calcination	ORR; Acetylene hydrochlorination	[20]
N-doped Graphene/ carbon black	Co_1 Ru_1 Pt_1	Iyophilization-annealing; Impregnation-calcination;	HER; CO_2 reduction; ORR;	[21]

C_3N_4	Pd_1 Pt_1 Co_1	Deposition-precipitation; Impregnation-calcination; Iyophilization-annealing;	Hydrogenations; Photocatalytic H_2 Evolution; Visible-light CO_2 reduction; ORR; OER;	[22]
ZIF-67 derivatives	Co_1	Hydrothermal method-pyrolysis; Dielectric barrier discharge plasma treatment;	ORR; OER;	[23]
ZIF-8 derivatives	Fe_1 Ni_1	Hydrothermal method-pyrolysis; Precipitation-pyrolysis;	ORR; CO_2 electroreduction;	[24]
UiO-66 derivatives	Ru_1	Impregnation-calcination	Hydrogenation of Quinoline	[25]
Porphyrinic Triazine-based frameworks	Fe_1	Ionothermal synthesis- pyrolysis	ORR;	[26]
Cu particle	Pd_1 Ni_1	Galvanic replacement method; Incipient wetness coimpregnation method;	Hydrogenation of butadiene to butenes; Selective hydrogenation of phenylacetylene; Semihydrogenation of acetylene; Non-oxidative dehydrogenation of ethanol to acetaldehyde;	[27]
Ni/Fe layered double hydroxides (LDH)	Au_1	electrodeposition method	OER	[28]

2.1.1 Metal oxides

The study of metal particles on oxide supports have received intensive attentions in heterogeneous catalysis, owing to the key role of the nature of the interaction of a metal particle with an oxide support in catalytic activity and selectivity.[1, 29] Low-index oxide facets of oxide supports are conducive to adsorption of metal catalyst, such as $CeO_2(111)$[30] and Fe_3O_4 (001),[31] in which the surface cation vacancy structures render extraordinary thermal stability of precious metal adatoms and prevent them agglomeration into clusters at high temperature

(700 K).[32] The support with oxidic defects is preferred with surface oxygen anions and OH^- groups as ligands, which lone electron pairs on oxygen for dative coordination and lead to the stronger interaction of unsaturated surface centres with isolated metal species, such as on ZnO,[11, 33] MgO,[34] Fe_2O_3,[33] Al_2O_3,[33] and TiO_2.[35] To design SACs, it is crucial to select a support which allows creation of defined metal sites on the surface and inhibits the aggregation of the metal atoms toward nanoparticles. A single metal atom could substitutionally replace a surface cation of a metal oxide support, stabilizing the single metal atoms via a charge-transfer mechanism. Many studies suggest that surface defects of oxide-supported metal clusters could provide anchoring sites for metal clusters and even single atoms.[36] The single metal atom might strongly anchor into the support due to its interaction with the neighbouring oxygen anions in a form of metal-O-support bonding, leading to the realization of isolated single atoms. Moreover, the metal-metal interactions between the adatom metal and the support metal can partially determine metal atom adsorption energy as well.

2.1.1.1 Low-index oxide facets as single-atom absorption sites

CeO_2. Ceria (CeO_2) surfaces with a limited amount of low coordinated surface sites can adsorb noble metal atoms and remain them stable in real reaction conditions.[30b, 37] Via the density functional theory (DFT) simulation (Figure 2a), Bruix *et al.* selected the cuboctahedral $Ce_{40}O_{80}$ nanoparticles as a representative model of nanostructured ceria, which features a truncated octahedral shape with O-terminated (111) and a fraction of (100) nanofacets. The (100) surface is much less stable than the (111) surface of ceria.[38] They identified (100) nanofacets as an effective surface to achieve atomically stabilized dispersion without bulk diffusion. The Pt^{2+} ($d8$) ions are well confined in square O^{2-} surface pocket at a (100) nanofacet of CeO_2, forming a square-planar PtO_4 unit as a Pt^{2+}-containing moiety. The theoretical calculation speculated that the adsorption energy of the anchored Pt_1 is high enough to withstand thermally-induced agglomeration into large nanoparticles and activity loss by diffusion into the CeO_2 bulk.[37]

Dvorak and colleagues emphasized the importance of defect sites on oxide support for single-atom catalyst stabilization. They realized the single Pt^{2+} dispersion at the step edges of highly defined monolayer ceria (111) surfaces. Jones and colleagues found that conditions under which nanoparticles emit mobile species are ideal to form single atoms if the mobile species can be effectively captured. Initially, a vapor-phase was utilized to transfer Pt from a metal foil to alumina.[39] As shown in Figure 2b, when the Pt/La-Al_2O_3 was physically mixed and sintered at 800 ^oC in flowing air, the ceria rods and polyhedrals can similarly trap the mobile Pt at the surface to effectively suppress sintering. In contrast, the cubic CeO_2 shows the lowest reactivity. They demonstrated that the Pt single atoms were randomly anchored on the ceria surfaces without any preference for specific facets. Atom trapping is feasible for preparing single-atom catalysts, which requires a supply of mobile atoms, a support that can bind the mobile species, and reaction conditions that are favourable to Ostwald ripening.[7c] Qiao *et al.* prepared two CeO_2-supported Au SAs with loading ratio of 0.05 wt. % Au by a simple adsorption strategy, which was denoted as $0.05Au_1/CeO_2$. The atomic high-angle annular dark-field scanning transmission electron microscopy (HAADF-STEM) images showed that Au_1 atoms were situated on the Ce columns of CeO_2 nanocrystallites (Figure 2c), implying that the Au_1 atoms were very likely anchored onto the surface Ce vacancy sites.[7a] Most recently, Li's group revealed that Au_1 prefer to anchor at CeO_2 step sites rather than terrace surface or on Au NPs (Figure 2d). For CO oxidation, they found that Au_1 exhibit little redox coupling with the irreducible support and only weakly bind CO; but the positively charged Au^+ could be formed due to the strong coupling with the reducible support, leading to vastly stable CO adsorption.[40]

2.1.1.2 Oxidic defects as single-atom absorption sites

Al_2O_3. Various modification has been made on Al_2O_3 to accommodate single atoms, such as porous Al_2O_3, θ-Al_2O_3, and γ-Al_2O_3.[8] Noble metals, such as Pt and Au, have been successfully trapped on these Al_2O_3 based materials. It was reported that the single atoms, like Pt_1, can be

anchored in the inner surface of the support, allowing these atomic species stable under oxidative and reductive atmospheres at high temperatures. It is believed that these trapped single atoms can modify the inert Al_2O_3 and show exceptional catalytic performance.[8a] Significantly, they developed a modified sol-gel solvent vaporization self-assembly method (Figure 3a), which spontaneously assembled into a highly ordered, hexagonally arranged mesoporous structure with Pt precursor encapsulated in the matrix.[8b] Besides the single Pt atoms, Au single atoms modified the inert Al_2O_3. It is found that the aluminium oxide clusters can react with single atom Au, attracting O_2, forming $AuAl_3O_3^+$, $AuAl_3O_4^+$, and $AuAl_3O_5^+$ cluster under thermal collision conditions. The attracted O_2 molecular on the gold-aluminium bond plays a key role on the catalytic oxidation of carbon monoxide (CO). Specifically, the extra O atom on the $AuAl_3O_5^+$ clusters make the Au-Al bond cleave and release valence electrons, which reduce oxygen and break the O-O bond, assisting to improve the cycling performance of CO.[8e] These results indicate that Al_2O_3 support is very vital to form unique active bonds with these single atoms in the oxidized catalytic reaction.

FeO_x. As early as 1999, Boccuzzi *et al.* reported that $FeO(OH)_x$ surfaces are necessary for the preparation of active Au_1/FeO_x catalysts.[41] Qiao *et al.* pioneeringly reported the synthesis of sing-atom Pt supported on iron oxide (Pt_1/FeO_x) via a co-precipitation method. The Pt loading ratio is 0.17 weight percent (wt. %). The low Pt loading ratio and high surface area of FeO_x nanocrystallite support simultaneously promote the isolated single atoms dispersion. A serial of the-state-art-of techniques are exploited to discern the only dispersion of isolated Pt, including aberration-corrected high-angle annular dark-field scanning transmission electron microscopy (HAADF-STEM) images and X-ray absorption (XAS) spectra. As displayed in Figure 3b, the HAADF-STEM images visually show the dispersion and configuration of Pt_1, Ir_1, and Au_1 single atoms (marked by the white circles) on the surface of FeO_x supports.[2, 9b, 42] For Pt_1/FeO_x catalyst, they demonstrated that the structure defects and the hydroxyl groups

derived from poorly crystallized and large-surface area FeO_x support plays a critical role in stabilizing the Pt single atoms. Furthermore, extended X-ray absorption fine structure (EXAFS) and X-ray adsorption near-edge structure (XANES) spectra in Figure 3c were measured and analysed to reveal the presence of Pt-O coordination and the positive charges of Pt single atoms due to the SMSI effect between Pt and FeO_x support. They concluded that the electron transfer from Pt atoms to the FeO_x surface leads to the positive charge of Pt atoms; The strong electrostatic and covalent interactions between high-valent single Pt atoms and the FeO_x surface are responsible for the stability of the single Pt atoms on the FeO_x support, ultimately accounting for the excellent catalytic activity of the Pt_1/FeO_x catalyst on CO oxidation.[2]

TiO_2. Defects on reducible oxide, such as TiO_2, can stabilize atomically dispersed metal atoms and attract researchers to develop various strategies of doping single noble atoms. Alternatively, Phillip's group used these ultra-refined nanosized TiO_2 particles (~5 nm) to separate Pt atoms via depositing precious metal atom on each TiO_2 particles to prevent the agglomeration. To use different ratio of additive, the Pt atoms were successfully loaded on TiO_2 particles with morphology of single atom, clusters, and particles. This work provided a characterization approach to evaluation the catalytic activity of each Pt single atom site, that is, using the correlated scanning transmission electronic microscopy (STEM) imaging and CO probe molecule infrared spectroscopy (IR), the strong IR signatures of CO bound from Pt single atoms shows a two-fold great than these Pt peroxided clusters.[10b] Besides the coordination of single atoms on TiO_2, He's group demonstrated that Au single atoms can be obtained via the reaction between Au^{3+} with TiO_2, forming $AuTi_2O_5^-$.[43]

Other absorption sites. Besides these popular metal-oxides based substrates mentioned above, variety of other metal oxides, including manganese oxide (MgO),[44] vanadium oxide (VO_2),[45] amorphous silica (SiO_2),[46] and tungsten oxide (WO_x),[16] have also been realized that can use for coordinating single atoms. For instance, ZnO NWs consisted primarily of (1010) facets

were utilized for the single Pt_1 and Au_1 atomic dispersion. The single atoms were identified to anchor at the surface Zn lattice sites and stabilized by the lattice oxygen. Moreover, the theoretical calculations confirmed that the coordination binding between single precious metal atoms and oxygen can largely enhance the reaction activity, and change the reaction selectivity.[11] Wang *et al.* reported a $ZnZrO_x$ support by incorporating ZnO to modulate the acidity of the ZrO_2 surface, which could provide more binding sites for atomic gold and much better stabilizes them against growth than either of the neat oxides.[12] Significantly, hollandite-type manganese oxide nanorods (HMO) can insert with Ag chains to expose the terminal Ag site, forming Ag single atom. This strategy was elaborately designed with the amount of Ag to open the HMO tunnels to expose catalytically active sites of Ag atoms.[13]

2.1.2 Nitrogen contained carbonaceous supports as single-atom absorption sites

It is ideal to utilize carbonaceous supports in SACs with the viewpoint of low cost. Direct single-atom adoption on graphene by ion implantation is of limited success. Meanwhile, the strong covalent C−C bonds render a substitutional doping by diffusion less efficient and compatible with tight thermal budget.[47] Thus, utilization of surface uncapped sites or aggregation inhibitors on the carbonaceous supports is vital to successfully stabilize the single metal atom species. Several reports have achieved single-atom doping on graphene *via multi*-step procedures with complex graphene modifications and inaccessible loading techniques, such as Pt_1, Co_1, In_1, Pd_1, and Ni_1.[19] Additionally, the single-atom niobium and gold realized atomically dispersion in graphitic layers of carbon.[20] Since the anchoring sites on the C supports are acquired with limit but not always abundant, which is prone to result in extremely low concentrations of single metal atoms, thus depriving the general utilization of this type of support.

Nitrogen-doped graphene/carbon. It is ideal to atomically disperse single atoms on thin two-dimensional substrate, which represents the ultimate low-end limit for SACs, exposing the most active sites with enlarged active surface area. Practically, nitrogen-doped graphene with rich anchoring sites and ideal 2D graphitic framework served as the most accessible support. As shown in Figure 4a, Tour's annealing graphene oxide (GO) and small amounts of Co, Ru, and Fe salts in a gaseous NH_3 atmosphere.[21a, 21b, 48] A hybrid with atomically dispersed Co onto nitrogen-doped graphene (Co_1-NG) was obtained (Figure 4b), which showed that the Co_1-NG possessed the similar morphology to graphene without any particles. The presence of Co_1 atoms was confirmed by the bright dots. They performed EXAFS analysis at the Co *K*-edge. The wavelet transform (WT) analysis (Figure 4c) indicated that Co single atoms are in the ionic state with nitrogen atoms. Hence, nitrogen doping on the graphene could serve as sites for Co atomic dispersion. The maximal efficiency of Co SAs enables the Co_1-NG as a highly active and robust HER catalyst in both acid and base media. Combined with the low-cost and scalable preparation method, the Co_1-NG is expected to be a promising candidate to replace Pt for water splitting applications.[21a] For the Ru_1-NG, the EXAFS Fourier transforms and WT in Figure 4d displayed the signal at ~1.5 Å and one WT intensity maximum at 5.4 $Å^{-1}$, which are associated with the presence of Ru-N(O).[21b] Meanwhile, atomic Fe single atoms and clusters on NG (Fe_n-NG) was fabricated via the similar process, which was estimated for CO_2 reduction to CO (Figure 4e). With Fe-N_4 moieties embedded in N-doped graphene. The high selectivity and activity of CO_2 to CO is ascribed to the synergetic effect of the Fe-N_4 moieties and N-doping on the graphene surface (Figure 4f).[48] In addition, Li's group demonstrated a serials of metal single atoms (M_1, M=Fe, Co, Ni, FeCo, FeNi) on nitrogen-doped carbon materials via carbonization of various polymers, including polydopamine (PDA), polyaniline (PANI), and polypyrrole (PPy).[49]

Metal organic frameworks-derived nitrogen-doped carbon. It remains challenges to fully control the synthesis of well-defined isolated atoms. Because the concentration of metal atoms is supposed to be extremely low to avoid aggregation, especially on the incorporated support. A strategy considered to solve this situation is to assembly organic ligands, which is expected to anchor single atoms and show thermal stability. It is believed that MOF structure is the best option, owing to the easy accessibility and numerous ligands dispersed on the architectural structures. It is well known that metal-organic frameworks (MOFs) are consisted with metal-containing nodes and organic linkers, in which the metal sites are atomically dispersed. Direct pyrolysis of MOFs are expected to be an ideal route for preparing various single atoms based on the versatility of metal ions and ligands. However, this approach is highly challenging due to the high-temperature pyrolysis tends to rapidly convert single-atom metal ions into aggregated nanoparticles. Li's group has made significant breakthrough on this direction, in which they utilized low-boiling-point Zn atoms (mp: 420 ^{o}C, bp: 907 ^{o}C) as a template so that to free abundant N-rich defects after Zn evaporated at high temperature. As a result, another metal can closely anchored through N-coordination to form isolated metal single atoms without aggregation during pyrolysis.[50] Specifically, as illustrated in Figure 4g, a ZIF-67-like Zn/Co bimetallic MOF (BMOF) was synthesized, in which Zn^{2+} replaced a certain proportion of Co^{2+} sites, thereby expanding the distances of adjacent Co atoms. The Zn^{2+} ions can be used as separators to adjust the distance of adjacent Co atoms and prevent the formation of Co-Co bond. Also, the leaving Zn^{2+} sites generate free N sites during pyrolysis, which can further provide thermal stability for these active single atoms. The single atom Co nodes are in-situ reduced and anchored into the nitrogen-doped porous carbon with Zn evaporated at high temperature. It is impressive that the Co loading ratio is as high as 4 wt. %.[23a] Furthermore, zeolitic imidazolate frameworks (ZIF-8) served as an effective precursor for the synthesis of Fe and Ni single atoms in N-carbon matrix (Fe-SAs/CN and Ni-SAs/CN).[24] $Fe(acac)_3$ and $Ni(NO_3)_2$

were selected as metal sources, which could be trapped into molecular-scale cages of ZIF-8 with cavity diameter (d_c) of 11.6 angstrom and pore diameter (d_p) of 3.4 angstrom. As illustrated in Figure 4h, after pyrolysis at 1000 °C under Ar atmosphere, ZIF-8 transformed into nitrogen-doped porous carbon with the evaporation of Zn. Meanwhile, $Ni(NO_3)_2$ within the cage were reduced by carbonization of the organic linker, leading to the formation of isolated single iron atoms anchored on nitrogen species.[24a] All MOF-derived single atoms showed superior electrocatalytic activities, owing to the synergistic effect between transition metals and N species, which will be discussed in details later. The broad range of ligands on MOFs has variety of selectivity. For example, the numerous free amine groups ($-NH_2$) at the skeleton of UiO-66-NH_2 are considered as a critical role to access the atomically isolated dispersion of single atom sites of Ru. It is suggested that Ru metal ions can be adsorbed within the MOFs channels by the strong coordination interaction between the electron lone pair of nitrogen and *d*-orbital of Ru atoms. The successful synthesis of single atom material and applications on catalytic reaction via coordination of organic ligands attracts more investigation on MOFs structures. Wang's group reported a feasible method to produce coordinative unsaturated metal sites through dielectric barrier discharge plasma treatment.[23b] Also, Cao's group reported that the atomic Fe species can be anchored on porous porphyrinic triazine-based frameworks (FeSAs/PTF) with a high loading of 8.3 wt. %.[26] Most recently, Zhang's group produced single-Co-atom catalysts via pyrolyzing Fe-Co prussian blue analogue followed by acid leaching. They utilized Fe doping and different calcination temperature to modulate the contents of pyrrolic N in the obtained N-doped graphene shells, which are favourable to form abundant CoN_4 sites (Figure 4i).[51] Thus, the strategy of using MOFs structure as substrates has been proved that it can effectively coordinate with variety of atoms with a high loading mass (>1 wt. %), indicating its easy control and huge potential for broader applications. Also, graphitic carbon nitride (g-C_3N_4) consists of 2D conjugated planes packed together with tri-*s*-

triazine repeating units through interlayer van der Waals interactions with lattice-hole structure. The characteristic N-coordinating cavities formed by the tri-*s*-triazine structure serve as potential scaffold for firmly anchoring isolated single atoms. Stable single-site Pd species was strongly trapped into the six-fold cavities of mesoporous g-C_3N_4, which offered the first stable single-site heterogeneous catalyst for hydrogenations of alkynes and nitroarenes.[22a] Li *et al.* successfully dispersed isolated single Pt atoms on g-C_3N_4 with loading amount of 0.16 wt. %. Since g-C_3N_4 itself is a promising stable and active catalyst for photocatalytic water splitting,[52] the Pt_1/g-C_3N_4 represents a new and highly efficient photocatalytic system for H_2 evolution.[22b] Qiao's group developed a range of molecule-level g-C_3N_4 coordinated single Co atoms (Co_1/g−C_3N_4) as a new-generation catalysts for these oxygen electrode reactions, including ORR and OER in alkaline media.[22c]

2.1.3 Organic ligand modification

The organic ligand on reducible oxides, such as TiO_2, can stabilize atomically dispersed metal atoms. It attracted researchers to develop various strategies of modifying surface of the supports. For instance, it has been reported that the ethylene glycolate (EG)-stablized ultrathin TiO_2 nanosheets can uniformly load Pd single atoms with a high ratio of 1.5 wt. %.[10a] In addition, it was reported that there are some other organic group can be used to modify the carbon, showing a strong interaction with single atoms. Yan's group demonstrated that the phosphomolybdic acid (PMA)-modified active carbon stabilized the Pt single atoms with a high Pt loading mass (close to 1 wt. %). It shown that the same loading mass of Pt atoms was severely aggregated without the modification of PMA, forming particles. The thermodynamic and kinetic control were considered as the key role to successfully synthesize single atom materials, that is, the various sites can provide vacancy to accommodate Pt atoms and the kinetic barrier of agglomeration for atoms anchored on spatially separated PMA species is substantially higher than those on support without modification.[53]

2.1.4 Metal supports

One alloying method has been developed to stabilize the single atoms with another metal to form an alloyed SAs, in which one metal is completely isolated by the second one.[54] By virtue of the synergistic effect of the bimetallic catalysts, the alloyed SAs exhibit geometric and electronic structures different from those of the single atoms that was prepared by anchoring on the support. Peng *et al.* successfully doped isolated Pt atom on gold particles via decreasing the loading mass of Pt species.[55] Sykes's group has done significant contribution in this system by both theoretical model and real catalytic experiments. As revealed via the scanning tunnelling microscopy (STM), Figure 5a clearly displayed rumpled appearance of the upper terrace, indicating Pd preferentially alloys into the Cu(111) surface above the step edges. The atomic resolution of the Pd/Cu alloy on the upper terrace (inset) shows the isolated Pd atoms in the surface layer appearing as protrusions. They found that a single atom alloy, with individual Pd atoms in a Cu(111) surface, could show lower energy barrier for both hydrogen dissociation and subsequent desorption (Figure 5b and c).[27a] As shown in Figure 5d, the concentration of the Pd relative to the host Cu surface is critical. When the Pd coverage is low, Pd could exist in the form of individual, isolated atoms into the Cu surface layer. The larger scale bar image in Figure 5e indicates that the alloying site is the ascending step edges. When Pd coverages increase, Pd islands could be observed on the surface as seen in Figure 5f and g.[27b] By the same method, they also synthesized Cu-alloyed Pd single atoms supported on Al_2O_3 via the galvanic replacement method.[27c] More recently, Pei *et al.* successfully synthesized silica gel supported Cu-alloyed Pd SAA by a simple incipient wetness coimpregnation method (Figure 5h). The IB-metal-alloyed Pd SACs were also systematically prepared with Cu-alloyed Pd SAC, in which similar active sites and catalytic mechanisms were revealed for the three catalysts.[27d] Similarly, it is reported that a trace amount of Ni was employed to atomically disperse on Cu particles forming NiCu alloy (NiCu SAA).[27e]

2.1.5 Metal sulphides, nitrides, and carbides

MoS_2. In some case, though the single atoms are not catalytically active, they unexpectedly play important role in enhancing the catalytic activity of support. Liu *et al.* reported atomic Co dispersed on MoS_2 monolayers, in which the Co-doping create many sulfur vacancy sites in MoS_2 basal planes.[17b] Bao's group reported that Pt_1/MoS_2 was synthesised by a one-pot hydrothermal method, leading to the formation of flower-like 2D MoS_2 nanosheets with uniform dispersion of bright Pt SAs.[17a]

TiC and TiN. TiN and TiC were considered as promising candidates for the metallic support material in PEMFCs, and methanol direct fuel cells, demonstrating clear advantages over traditionally used acidic susceptible carbon-based supports, including good electrical conductivity and its high resistance to corrosion and acid attack. In a view of combination of the high-efficiency single atom material and stable TiN, Soon's group developed a theoretical strategy to anchor Pt single atoms via producing N-vacancy on the surface. Comparing to the clean TiN surface, TiN surface vacancies is energetically favourable of Pt atoms. The author also further shown the charge density differences, when Pt bonded with N vacancies and Ti vacancies. For the N vacancy, it demonstrated that Pt atoms embedded into the TiN surface experiences a significant increase in the occupation of the 5*d* states due to coordination by the four neighboring surface Ti atoms, where the electronegativity of Pt (Pauling value of 2.28) is large than that of Ti (Pauling value of 1.54). For Pt atom adsorption on Ti vacancies, the charge redistribution is directional and both N and Ti atoms are involved in the charge transfer, leading to the depletion of the planar Pt 5d states and the unfavourable Pt adsorption energy.[18b, 56] Via DFT calculation, Back *et al.* explored a range of SACs, where transition-metal atoms (M=Ag, Au, Co, Cu, Fe, Ir, Ni, Os, Pd, Pt, Rh, and Ru) are doped at surface defect sites of TiC and TiN. The iridium-doped TiC (Ir_1@*d*-TiC) was theoretically evaluated as highly active and selective CO_2 reduction catalysts.[57]

2.2 Support effects for stabilizing single atoms

Single metal atoms are in principle easier to aggregate than metal NPs, and thus SMSI are required for the thermal stability of SACs. Campbell and his co-workers found that small particles have a much lower heat adsorption than large particles, indicating the lower onset temperature for Ostwald ripening.[58] Moreover, they measured the energies of Ag atoms in Ag NPs supported on CeO_2 and MgO surfaces, which demonstrated that Ag NPs with any sizes below 1000 atoms had much higher stability on reduced CeO_2(111) than on MgO(111). This effect was found to be a result of strong bonding to both defects and CeO_2(111) terraces (Figure 6a).[59] Qiao *et al.* reported that the Au_1/FeO_x catalysts were not only highly active but also extremely stable, even at temperatures as high as 400 °C; they proposed the single Au_1 atoms located at Fe vacancy sites of the FeO_x nanocrystallites via strong covalent metal-support interaction (CMSI), thus immobilizing the Au_1 atoms on the support surface.[9b] Additionally, atomically dispersed Au on FeO_x supports also were proven to show a remarkable stability in heat treatments up to 500 °C.[60] Inspired by these works, Li *et al.* investigated the catalytic properties of various single-atom catalysts M_1/FeO_x (M = Au, Rh, Pd, Co, Cu, Ru, and Ti) by means of DFT computations, which shed light on developing superior catalysts for CO oxidation. As illustrated in Figure 6b, the most stable sites for all the single metal atoms are vacancy-free 3-fold hollow sites, which induced significant charge transfers from the single-metal atoms to iron-oxide surface. The DFT calculation verified that the high stability could be indicated by the strong binding energies and diffusion barriers of the single-metal atoms on the FeO_x support. Generally, oxygen vacancies are inevitable, in which the binding strengths of the single metal atoms to the less coordinated oxygen (two M-O bonds) are weakened and the electron transfers from metal atoms to the surface are reduced as well.[61]

Furthermore, the co-doped nitrogen can stabilize these metal atoms from aggregating to form metal particles. Typically, there are three types of N in the N-doped C, including graphitic-N,

pyrrolic-N, and pyridinic-N.[25, 51, 62] The pyrrolic-N and pyridinic-N are located in a π conjugated system,[63] and their p-electrons are believed to stabilize metal single atoms. In order to understand the electronic and structural properties between single metal atoms and N-doping supports. X-ray absorption spectroscopy (XAS) has been utilized to probe metal-support interface. For the Pt_1, Liu *et al.* found that individual Pt single atoms could be homogeneously anchored on N-doped carbon black (N: 2.7 wt. %). In contrast, when the carbon support without N-doping, besides the Pt_1 atoms, Pt nanoparticles co-existed as well with the same Pt loading ratio (0.4 wt. %) and synthesis procedures. This result indicated that the N-doping of carbon support plays a critical role in effectively anchoring Pt_1 atoms and prevent their aggregation. As illustrated in the Figure 6c, the pyridinic (P)-N has been identified as the strong anchoring sites for Pt single metal atoms due to the modified interfacial interaction. The adsorption energy of Pt_1 on g-P-N_1 is -5.35 eV, which is much lower than that on pristine graphene (-1.56 eV). This suggests that the Pt_1 can be selectively trapped strongly by g-P-N_1 site and thus improve and stabilize the dispersion of Pt single atoms on N-doped graphene surface, confirming the vital role of support properties on the formation of single atoms.[21c] Recently, Li's group achieved a high Pt_1 loading ratio up to 5.3 wt. % on N-doped graphene via a Na_2CO_3 salt-assisted one-pot pyrolysis strategy.[62] A main peak at 1.61 Å in the FT-EXAFS curve for this sample corresponds to Pt-N coordination and can be further calculated to be Pt-N_4 configuration (Figure 6d). On the N-graphene support, Ru-N_4 moieties are represented by a porphyrinic or pyridinic geometry (Figure 6e).[21b] The ZIF-8-derived Fe_1/NC and Ni_1/NC, and Zn/Co-ZIF-67-derived Co_1/NC show a 4, 3, and 2 metal coordination number with surrounding N atoms, respectively (Figure 6f).[23a, 24] With precise N-coordination, the high metal loadings of 1.5-4 wt. % is achieved. For the Ru_1/N-C from UiO-66-NH_2, the Ru loading ratio is only 0.3 wt. %, which corresponds a coordination environment of Ru-N(C_2) in Figure 6g.[25]

3. Electronic structure due to atomic-local environments

The foreign atoms implanted on a specific support could change the electronic structures. These changes are based on the field of condense matter physics and will result in the materials features in a vast array of practical applications. However, the electronic structures are affected over the type and quantity of dopants. Recently, tremendous types of metal atoms have been employed as dopants in atomic level and investigated through attaching with various host materials, including metal compounds, carbon, modified carbon, and nano-sized metal particles over the years.[64] The different local structure of these substrates provides alternative coordination environment and electronic correlation with atomic dopants. These effects play an essential role in a wide range of applications and must be investigated in advance. We summarized the change of electronic structure with showing how the metal atoms can be tuned by the different physical properties of the host materials. The different host materials provide varieties of local structures due to the change of thickness, phases, and strains. The alternation of the local environment of foreign atoms arise a series of differences of the surface engineering, such as orbital exchange-coupling interaction, the electronic band gap, electron density, and adsorption energy. Fako *et al.* checked the electronic properties of the same Pt single atoms on the matrices of oxides, metals and carbon nitride. By computing the d-band center of Pt and studying the DOS, they confirmed that the degree of metal-support overlap and electron sharing relied strongly on the host materials. It was observed that the Pt *d* and *s* states are completely mixed with those of Cu over a broad range of energies with d-states shifted 0.47 eV towards negative values with respect to the Pt bulk. The d-states of Pt were depleted in the top of the valence-band of the Fe_2O_3, which were less available for bonding. In contrast, Pt_1 on g-CN seemed to show isolated nature of SACs with almost separated energy levels while the aromatic rings in the g-CN might show strong effect on the properties of the Pt centers.[64] Thus, the theoretical predictions have many times confirmed that the heterogeneous dopants hugely affected the local structure of host materials, changing their performance in various potential

applications as well. It is of highly significance to prepare these promising single-atom based materials in the real use. Fortunately, researchers have developed ways to achieve these ideal single atom structures through considering the unique properties of varieties of supports, such as metal oxide, carbon, modified carbon, and metal particles.

3.1 M_1-metal oxides

It is of high significance to understand the electronic environments of atomic dopants on metal oxide. Recently, Senftel's group has systematically investigated the metal-support interactions via anchoring a range of transition metal single atoms (Cu, Ag, Au, Ni, Pd, Pt, Co, Rh, Ir, Fe, Ru, Mn and V) on several common reducible and irreducible oxide supports (CeO_2(111), MgO(100), CeO_2(110), TbO_2(111), ZnO(100), TiO_2(011) and α-Al_2O_3(0001) surfaces).[65] They concluded that the adsorption sites of single-atom transition metals on metal oxides supports includes threefold hollow sits, twofold oxygen bridge sites, oxygen side-bridge sites, and anionic oxygen sites. For example, based on energetically favourable configurations, Ag is favourably adsorbed at a threefold hollow site, Ir is bonded at a twofold oxygen bridge site, while Pd is located at an oxygen side-bridge site on the CeO_2(111) substrate (Figure 7a); In contrast, all metal single atoms are adsorbed above the anionic oxygen on the MgO(100) surface (Figure 7a). The adsorption energy of a metal atom onto an oxide surface in Figure 7b showed a linear trend against the adsorbed metal's oxide formation enthalpy, suggesting that the presence of metal-oxygen-metal bonds formed.[65] Also, it is noticeable that the support itself plays a role in determining the overall metal binding strength, since the trend of metal adsorption strength on each support surface shows a distinct slope. To better understand the electronic mechanism of SMSIs, they simulated the electronic structures of two metal atoms with two oxide support: low oxygen affinity Ag and high oxygen affinity Ir and reducible CeO_2(111) and irreducible MgO(100). As illustrated in Figure 7c, significant charge transfer takes place between Ir and the surface, which results in the charge redistribution from Ir adatom

towards neighbouring oxygen and cerium atoms, thereby the formation of an Ir^{2+} states. As displayed in the corresponding density of state (DOS) plot, it is interesting that a peak just above the Ce-O bond was observed, which confirmed a charge accumulation in a metal-metal hybrid orbital. Beyond the typical metal-oxygen-metal interactions, these results reported the metal-metal binding between metal adatoms and metal oxides, which should be take into account in SMSI as well. Figure 7d demonstrates that the charge transfer between Ag and CeO_2 (111) are less, only forming an Ag^+ state by reducing one Ce atom. By comparing the charge density difference plots of $Ir_1/CeO_2(111)$ and $Ag_1/CeO_2(111)$, green band linking Ir and Ce atoms is observed, which indicated a charge accumulation and revealed the presence of metal-metal binding. For the irreducible MgO (100), it is unable to readily accept electron density from a metal adatom but instead reduces the metal adatoms. The metal-support interactions are localized onto one surface oxygen via transferring electron density from the support to the adsorbed Ir (Figure 7e). Moreover, some researchers systemically examined various SACs with metal oxide supports towards a specific catalytic reaction, such as CO oxidation,[40, 61, 66][67] thus guiding to design more efficient and cost-effective heterogeneous catalysts. For instance, Li *et al.* simulated a serials of promising CO oxidation catalysts by anchoring metal single atoms on FeO_x, including oxygen-defective M_1/FeO_x (M = Au, Rh, Pd, Co, Cu, and Ru) and vacancy-free M_1/FeO_x (M = Au, Rh, Pd, Co, Cu, Ru, and Ti) surfaces.[61] All the SACs showed very higher stability and better overall catalytic performance than the highly active Pt_1/FeO_x.[2] Followed the same Langmuir−Hinshelwood (LH) mechanism for the CO oxidation, the Ru_1/FeO_x stands out due to having very low activation energy in each step. In contrast, both Co_1/FeO_x and Ti_1/FeO_x exhibited very low activation energies for CO oxidation; while Au_1/FeO_x could be poisoned by CO. Yang *et al.* examined the CO oxidation of single-atom metals (M = Pd, Fe, Co, and Ni) on γ-Al_2O_3. According to the DOS of 2p orbitals of the surface O, the binding energies of Ni and Pd with Al_2O_3 bearing an Al vacancy are much smaller than

those of Fe and Co, which lead to lower oxidation state of Ni and Pd (+2) and poor bonding interactions with the neighbouring O atom. The high reactivity of Ni and Pd originate from the neighbouring O atom. they concluded that metals that tend to take a +2 oxidation state are good candidates for the single-atom catalyst M_1/Al_2O_3 for CO oxidation.[66a]

3.2 M_1-N_x-C_y

It is vital for future renewable energy technology to develop highly active SACs for electrochemical reactions. For CO_2 electroreduction reaction (CRR), Jung's group investigated a single transition metal atom (Ag, Au, Co, Cu, Fe, Ir, Ni, Os, Pd, Pt, Rh or Ru) anchored on defective graphene with single or double vacancies, denoted as M@sv-Gr or M@dv-Gr, respectively. As shown in Figure 8a, the top view of two atomic configuration has been displayed. The corresponding binding energies of M anchored on single or double vacancies were summarized in Figure 8a (bottom), which indicated that Co, Fe, and Rh were more stable to loading on the sv sites, while the rest of metals showed favourable and sufficiently strong binding with the dv-Gr sites. The results summarized in Figure 8b confirmed that most of M@sv-Gr and M@dv-Gr with high selectivity to form either *COOH or *OCHO than *H, which suggested that these single metal sites can be effective catalysts towards CRR rather than HER. They further concluded that the Pt@dv-Gr catalyst showed better reduction with CH_3OH production than any existing catalysts. In contrast, Ni@dv-Gr and Pt@dv-Gr showed high selectivity for CH_3OH production; Os@dv-Gr and Ru@dv-Gr preferred CH_4. Recently, Zhang *et al.* studied 34 SACs with defective graphene anchoring single heteroatom (IIIA, IVA, VA, VIA and VIIA), for oxygen reduction reaction (ORR). Similar geometric structures were employed for a serials of X-SV/DV (X =B, C, N, O; Al, Si, P, S; Ga, Ge, As, Se; In, Sn, Sb, Te; Tl, Pb, Bi). They summarized a "volcanic curve" relationship between ΔG_{OH^*} and energy barrier (Figure 8c). With the reaction pathway of $O_2 \rightarrow OOH^* \rightarrow O^* \rightarrow OH^* \rightarrow OH^-$, the Te-SV,

Sb-DV, Pb-SV, Pb-DV, As-SV, As-DV, B-SV, Sn-SV, and N-SV exhibited low reaction energy barrier of less than 0.8 eV.[68] Moreover, Zeng's group evaluated the activity of graphene-based single-atom catalysts towards the oxygen reduction, oxygen evolution and hydrogen evolution reactions (Figure 8d). They found that Fe-pyridine/pyrrole-N_4 is favourable for the oxygen reduction reaction; Co-pyrrole-N_4 is more suitable for the oxygen evolution reaction. Impressively, the Mn-pyrrole-N_4 showed higher activity towards the hydrogen evolution reaction than precious Pt/Ir/Ru-based catalysts, which suggested that macrocyclic metal complexes, especially the M-N-C-based SACs, could be used as an alternative to graphene-based single-atom catalysts.[69]

3.3 M_1-metal

SAA materials conduct selective catalysis by performing facile bond activations, which uptake species onto the surface and the subsequent spill over of adspecies onto the noble host material. Some groups have done multitude of modelling studies for guidance of different possible SAAs and better understanding reaction pathway of different reactions.[70] Stamatakis's group did a widespread investigation, which involved the fundamental adsorptive and catalytic properties of 12 SAAs (Ni-, Pd-, Pt-, and Rh-doped Cu(111), Ag(111), and Au(111)) for 5 catalytic reactions, including H_2 dissociation, CH_4 activation, NH_3 activation, CH_3OH dissociation, and CO_2 reduction. As shown in the Figure 9a**,** H_2, CH_4, NH_3, CH_3OH, and CO_2 are absorbed to the top site of all SAAs during initial state, including Ni/Cu, Pt/Ag, Rh/Cu, Ni/Ag, and Pd/Au. The following dissociation or activation followed a top-bound transition state. There is another "methoxy-like" transition state for CH_3OH absorbed on Pt/Cu, which is located at the host metal sites that are adjacent to the dopant single atom. Compared to the pure metals, the corresponding industrially relevant reactions were predicted in Figure 9b. They concluded that SAAs typically possess weak binding and low activation energies for bond dissociations in H_2, CH_4, and NH_3; SAAs also showed very low activation energies for the CO oxidation reaction

and CH_3OH dissociation in several cases. This large amount of data can aid the design and development of SAA materials towards specific catalytic reactions. For instance, RhAu SAAs would be a promising catalysis for activation of C−H bonds.[71] In addition, electronic structure changes typically involved a shift in the *d*-band position relative to the Fermi level. Thirumalai *et al.* calculated the *d*-band atom projected density of states (DOS) of the single atoms (Pt, Pd, Ni, Rh and Ir) in several representative host metals (Au, Ag, and Cu).[70a] A sharp feature close to the Fermi level was observed, which was ascribed to an ineffective mixing of the electron densities of the host metal and the single atom as well as due to an effective tensile strain on the single atom, responsible for the high surface reactivity. For water and nitric oxide dissociation, the high reactivity showcased by palladium alters the geometries of adsorbates by making them adsorb in close proximity to the Pd atom. This leads to a more exothermic and energetically favorable process for the adsorption of species, which in turn activating the reactant molecules more strongly. For the hydrogenation of acetylene to ethylene, they speculated an enhancement of adsorption at the Pd site, with an increased degree of selectivity, due to the more favourable energetics of adsorption.

3.4 M_1-Other supports

For instance, Li's group calculated the change of structural, electronic, and magnetic properties of MoS_2 through using a full range of substitutional dopants form non-metal to metal atoms. As shown in Figure 10a, both the non-metal and metal doping show more stable configurations compared with the pristine ones. The spin resolved densities of the non-metal substitutions (H, B, N, F) indicated that the spin polarizations are mainly localized on dopants and adhesive atoms, while the polarizations of metal substitutions (V, Cr, Mn, Fe, Co) are mostly localized on the metal atoms. Their band structures in Figure 10b indicated that the H substituted MoS_2 sheets were metallic for up-spin channel but semiconductor for downspin channel with direct band gap of 1.20 eV at K. In contrast, B and Cr substitution enabled the sheets behave as direct

semiconductors for up-spin channel and metals for downspin channel, with the corresponding band gaps of 1.61 eV at K and 1.15 eV at Γ, respectively. Also, DOS suggested that the impurity states of non-metal were hybridized between 2*p* states of non-metal atom and 4*d* states of nearest Mo atoms, rarely contribution from the 3*p* states of S atom. The impurity states of metal atoms, however, originated from both the 4*d* orbital of metal atoms and Mo atoms.[72] Bao's group reported that the catalytic activity of in-plane S atoms of MoS_2 can be trigged via single-atom Pt doping for hydrogen evolution reaction (HER). The triggering mechanisms of various metal SAs have been investigated via DFT calculations. As shown in Figure 10c**,** the metal atoms could substitute the Mo atoms in the MoS_2 matrix, leading to two different configurations of doped MoS_2. Some metal atoms, including V, Ti, Fe, Mn, Cr, etc., tend to remain in the middle to bond with six S atoms, which can be anticipated to possess low activity due to their weak binding ability with H. While other metal atoms, such as Pt, Ag, Pd, Co, Ni, etc., are prone to shift toward one side and bond with only four S atoms but with other two S atoms unsaturated, leading to distinctly high adsorption behaviours of H atoms on the two unsaturated S atoms and thereby high HER activity. It is clear the Pt-MoS_2 shows higher HER activity than Ni- and Cu-doped MoS_2, which are owing to the overly strong adsorption of H* by the unsaturated S atoms neighbouring the dopants (Ni and Cu) on the left side of the volcano plot.[17a]

4. Catalytic capability due to atomic-local environments

SACs can typically accelerate a wide range of reaction, such as CO oxidation,[2, 8a] methane conversion,[73] water-gas shift (WGS) reaction,[9a, 35] and other important reactions,[20a, 74] which could achieve orders of magnitude higher activity than their NP counterparts. For the WGS reaction, it is impressive that SACs on oxide supports are always more active than their NP counterparts based on turnover frequency (TOF),[9a, 14, 75] since the NPs only serve as spectators during the WGS reaction. It is noteworthy SACs are not omnipotent and even inactive,

especially for the catalytic reactions that require two or more neighbouring metal atoms to activate these conversions. Some SACs are inferior in catalytic activity than their NP counterparts for CO oxidation, Taking M_1/FeO_x as examples, when anchored on FeO_x support for CO oxidation. Pt_1 could deliver 2-3 times more active than Pt NPs;[2] Au_1 was comparable to its NP counterpart,[9b] while Ir_1 and Rh_1 are less active than their NP counterparts.[42, 61] For oxygen reduction reaction, the Pt_1 selectively followed an inferior two-electron pathway producing H_2O_2.[76] Certainly, it should be pointed out that the advantages of SACs are multifarious and not always limited to activity but depend on a variety of factors on a case-by-case basis.[2, 14, 77]

4.1 Activity

4.1.1 M_1-Metal oxide

To our knowledge, indirect references of single-atom catalysis on inert substrates are limited to parts of metal oxides, including the Al_2O_3, MgO, and SiO_2. On the other hand, those supports, which can provide active sites by themselves without any modification, are defined as active supports, including active metal oxides, carbonaceous structures, and metal particles. The earlier study suggested that the metal oxide supported metal particles (Au) can be grouped to two categories with respect to the CO oxidation, which dependent on the support materials and differ in the reaction mechanism. Catalyst loaded on inert supports is intrinsically less active, but significantly enhanced activity while supported on reducible transition metal oxide, such as Fe_2O_3.[78] Thus, it is important to separate the support effects as inert support and active support to have a deep understanding on the alternative interfaces.

4.1.1.1 M_1-Inert metal oxide

The inert support is commonly irreducible and non-active on catalytic reaction. Over the past decade, single atom doped inert support demonstrated their enhanced capability on oxidation

due to the electronic interaction with the inert metal/O terminate. This type of materials have attracted increased interests to investigate their fundamental mechanism.

Alumina as typical inert metal oxide has been commonly used as substrate to support single atoms. Typical noble metals, such as Pt, Pd, Rh, and Au, have been successfully trapped on these Al_2O_3 based materials, showing catalytic properties on CO oxidation, NO oxidation, and selective aerobic oxidation of allylic alcohols.[8a, 8b, 79] Although all recent studies proposed that these single atoms can be catalytic sites for the oxidized reactions, there still is a debate on while the single atom require the inert Al_2O_3 or not. Masahiro's group indicated that a considerable charge transfer from single atoms (Pd/Fe/Co/Ni) to Al_2O_3 support happens via using DFT calculation, as the Al has largest binding energy and positive charge.[66a] Also, it has been reported that Au single atoms on the inert Al_2O_3 attracted O_2, forming $AuAl_3O_3^+$, $AuAl_3O_4^+$, and $AuAl_3O_5^+$ cluster under thermal collision conditions. The attracted O_2 molecular on the gold-aluminium bond plays a key role on the catalytic oxidation of carbon monoxide (CO). Specifically, the extra O atom on the $AuAl_3O_5^+$ clusters make the Au-Al bond cleave and release valence electrons, which reduce oxygen and break the O-O bond, assisting to improve the cycling performance of CO.[8e] These results indicate that Al_2O_3 support is very vital to form unique active bonds with these single atoms in the oxidized catalytic reaction. Rh/Al_2O_3 also was successfully prepared[79a]. It turns out that the Rh-O was mainly contributed to the first CO oxidation, while the cleavage of Al-O bonds were involved in the second CO oxidation to eliminate the CO_2 (Figure 11a). These results consistently confirmed that both of the doped single atoms and supports attend the catalytic reaction and have active capabilities. However, Chaitanya's group proposed a quite different mechanism by showing the CO performance on sample Pt/Al_2O_3. It shown that CO_3 intermediate was formed in the oxidation of CO. The CO_3 species was only bonded to the single atom Pt and shown a difference with the previous study, which is reported that the CO_3 is bonded to more than one Pt atom via O

and C (Figure 11b). Such a proposed mechanism shows a facile pathway that the single atom can be catalytically active site without involving the inert substrate.[8a]

As we mentioned above, the inert substrate would not show intrinsic catalytic ability, except the impurities were doped on the surface to activate them. However, the different single atom dopants could have alternative effects due to the change on the electronic structures. To the better understanding of the electronic correlation between supports and single atoms, a systematic investigation should be taken to consider. For instance, Natalia's group compare the adsorption energy of single atom Pd and Au on MgO (001).[80] The result shown that The Pd single atom had a stronger binding energy than that of Au single atom. Another theoretical simulation also has been performed via DFT calculation to compare the CO activity trends of single atom catalysts on MgO (M/MgO, M = Cu, Ag, Au, Ni, Pd, and Pt). This systematic study indicated that only Ag, Cu, and Ni/MgO shown catalytic ability on oxidation of CO. Especially, Ag/MgO exhibit better catalytic performance than other single atoms.[66b]

4.1.1.2 M_1-Active metal oxide

M_1-FeO_x. It is readily comprehensible that the types of SACs directly determine the catalytic performance when anchored on the same support. Taking M_1/FeO_x as examples, when anchored on FeO_x support for CO oxidation. Pt_1 could deliver 2-3 times more active than Pt NPs;[2] Au1 is comparable to its NP counterpart,[9b] while Ir_1 and Rh_1 are less active than their NP counterparts.[42, 61] The catalytic activity for single atoms on the same FeO_x support show a trend with the order $Au_1 > Pt_1 > Ir_1 \approx Rh_1$, which is oppositely corresponding to the absorption strength of CO on metal sites because the weak CO adsorption is favourable and could significantly enhance the adsorption and activation of O_2 (Figure 12a). On the other hand, the stabilization of SACs and catalytic properties are closely related to the support effects. It is noticeable that surface of the FeO_x support is dominated by Fe_3O_4 with abundant oxygen

vacancies and hydroxyl groups, which are believed to provide reactive O atoms for the reactions and play critical roles in the oxidation reactions, especially for WGS and CO oxidation.[81] The impact of surface O atoms is revealed via in-situ spectroscopy that surface lattice O atoms of the FeO_x support could assist the single atoms to directly participate in CO oxidation.[82] *Via* a co-precipitation method, Ir_1/FeO_x catalysts were synthesised with loading ratio of 0.01 and 0.22 wt. %, which were denoted as $0.01Ir_1/FeO_x$ and $0.22Ir_1/FeO_x$, applying into water-gas shift (WGS) and CO oxidation, respectively. The $0.01Ir_1/FeO_x$ achieved one of the most active catalysts reported for water-gas shift WGS (Figure 12b). On the other hand, the 0.22 Ir_1/FeO_x was verified a higher energy barrier than Pt_1/FeO_x catalysts for CO oxidation, which is responsible for its lower activity. This work revealed the fundamental mechanism of isolated surface atoms and could contribute to design various single-atom catalysts with high activity.[9a, 42]

The active oxides have high intrinsic activity compared with inert metal oxides. It commonly sees that the catalyst of single atoms, which were doped on inert metal oxides, were utilized on oxidized reaction, such as CO oxidation. However, when the single atom doped on active metal oxide, they were broadly developed in various reactions, including reductive catalytic path. For example, catalyst Pt_1/FeO_x shown a high efficiency in the reduction of NO to N_2.[9c] Also, Zhang's group illustrated that single atom Pd_1 on FeO_x can be utilized as bifunctional catalyst, including the conversion of CO to CO_2 and dissociation of H_2O to form H_2. It is suggested that Pd single atoms greatly enhanced the reducibility of FeO_x and facilitated the formation of oxygen vacancies, which served as sites to promote the dissociation of H_2O to form H_2 and atomic O.[83]

M_1-TiO_2. If we use the TiO_2 as a prototype, the impurity doping or ion implantation on TiO_2 can narrow its wide band gap in order to create fascinating photocatalysts which is not only operated under ultraviolet (UV) light but also natural light. It has been found that the metal,

such as 3d transition metal (V, Cr, Mn, Co, Ni, Fe), doped TiO_2 can tune the localized structure and energy level. For instance, the dopants, including V, Cr, Mn, or Fe had the localized level of the t_{2g} state lying in the band gap, the Co was even situated at the top of the valance band (VB). However, the Ni dopants were rather delocalized, thus significantly contributing to the formation of the valance band with the O p and Ti 3d electrons.[84] Specifically, when the isolated noble-metal-atom, such as Pt, is grafted onto the high-energy facets (001), the interfacial charge transfer increase the density of localized electrons around the doped noble metals and lowers the work function.[85] As a result, the single atoms can efficiently receive excited electrons to generate surface-adsorbed hydrogen atoms (H*), facilitating the efficiency on H_2 evolution. Experimentally, it shown that Pt/TiO_2-001 presented a maximum H_2 evolution rate of 21.9 mmol $h^{-1}g^{-1}$. Similarly, the single atom Pd_1/TiO_2 also demonstrated a better hydrogenation, owing to the yields of $H^{\delta-}$ and $H^{\delta+}$.[10a] In addition, the accumulation of electron around single atom Pt on TiO_2 surface can effectively trap CO gas. Phillip's group illustrated that sample Pt_{iso}/TiO_2 had a strong IR signatures of CO bound from Pt single atoms shows a two-fold great than these Pt peroxided clusters.[10b] Besides the coordination of single atoms on TiO_2, He's group demonstrated that Au single atoms can be obtained via the reaction between Au^{3+} with TiO_2, forming $AuTi_2O_5^-$. The closed-shell gold containing heteronuclear oxide $AuTi_2O_5^-$ are reactive toward CO oxidation than the corresponding open-shell titanium oxide cluster anions (Figure 12c). The essential role of Au single atoms have been confirmed by theoretical calculations, indicating that gold atom can act as a CO trapper and electron acceptor.[43]

CeO_2. Impressively, when anchored on different shapes of the same supports or different supports, the same type of single atoms could exhibit different activity and selectivity. For instance, ceria with various shapes, including rods, cubes, and polyhedral, were utilized as supports of 1 wt. % Au. Gold was poorly dispersed and aggregated into nanoparticles when

deposited on the CeO_2 nanocubes (100), which was inactive for the low-temperature WGS reaction. In contrast, most of the gold on the (110) facets of CeO_2 nanorods was atomically dispersed with high activity. This results manifests that the (110) have more binding sites for gold than the (100) polar surfaces of CeO_2.[86] Meanwhile, the research on Pt_1/CeO_2 also confirmed the important role of surface O atoms. A steam treatment at 750 °C was conducted, which was expected to afford active surface lattice O atoms in the vicinity of Pt^{2+}, leading to high activity for low-temperature CO oxidation.[87]

In sum, the catalytic properties of a SAC are closely related to the atomic-local environments when anchoring on different supports. As illustrated in Figure 13a, various active oxide supports, including CeO_2, ZnO and FeO_x single crystal, are utilized to compare the substrate effect.[88] Boucher *et al.* found that ZnO (0001) surfaces are the favourable supports for the active Au sites toward water-gas shift (WGS).[88-89] It is evident that activation energy and conversion rates of the Au-FeO_x are lower compared to Au-CeO_2 and Au-ZnO for WGS reaction tests. The possible reason for the lower activity is a weaker interaction of the Au with iron oxide surface. They suspect an instability/deactivation of the Au–FeO_x nanoshapes under reaction conditions (Figure 13b). Moreover, the "shape effect" of oxide supports is examined for both WGS and MSR reaction. The WGS reaction of Au/FeO_x catalysts depends on the iron oxide shape in experiments with gold deposited on single crystals of nano-Fe_3O_4, (i.e., octahedra (111) and cubes (100), Figure 13b.[88] As shown in Figure 13c, both Au-CeO_2 and Au-ZnO are active catalysts for the MSR reaction. It is evident that Au-CeO_2 delivered higher reaction rates, which is attributed to the better dispersion of Au on CeO_2 (110) surfaces, leading to more Au-O active sites. This Au-O species serve as the active sites for methanol reactions, in which the CeO_2 (110) surfaces that can disperse gold atomically are also superior to CeO_2 nanocubes presenting (100) surfaces.[89-90] Au–ZnO samples with a large fraction of ZnO (0001) surfaces exposed (polyhedra and short rods) are

active for the MSR reaction (Figure 13c). Liu *et al.* carried out a systematic investigation on support effects via dispersing single Pt_1 on highly reducible Fe_2O_3, reducible ZnO, and irreducible γ-Al_2O_3. It was proven that Pt_1/Fe_2O_3, Pt_1/ZnO, and Pt_1/γ-Al_2O_3 are all active for CO oxidation and the reducibility of the supports determine the catalytic performance of Pt_1 SACs (Figure 13d and e). At 140 °C, the TOF value of that Pt_1/Fe_2O_3 is larger than that of the Pt_1/ZnO, which are much larger than that of Pt_1/γ-Al_2O_3. The TOF of a Pt_1 atom supported on Fe_2O_3 and ZnO is about 50 and 18 times higher than that of a Pt_1 atom supported on γ-Al_2O_3.[33] Such a huge difference in the TOF value of one Pt_1 atom suggests that that the interaction between single metal atom and support as well as surface properties of supports control the catalytic behaviour of SACs. This raises a question about how the single atoms supported on the inert substrates and active substrates work as catalytic sites.

4.1.2 M_1-N_x-C_y

Carbonaceous nanostructures are intensively used as supports to coordinate with boron, nitrogen and metal atoms since their rigid skeletons possess planar sp^2 molecular orbitals sandwiched between overlapping unsaturated delocalized electrons.[91] Also, the modified carbonaceous materials, which are functionalized by physisorption, impurity dopants and covalent bonding, have been widely used in molecular sensing, controlling, drug delivering, catalysts, and batteries.[92] Especially, developing stable metal-doped carbon nanostructures are highly attractive in catalytic applications. Interestingly, the host carbonaceous materials were strongly affected by the metal dopants in ground states, axial coordination, stability, electric field, spin and charge density. For instance, the different binding sites caused by metal dopants have different geometrical and electronic environment, because the distortion of metal atoms breaks the plane of symmetry and makes themselves unsaturated, binding with different types of ligands.[93]

Moreover, the applications of SACs are extended to electrocatalytic reactions.[94] Besides the requirements on the nature and number of active sites as these in thermocatalytic reactions, the activity of the catalysts in electrocatalysis additionally relies on the properties with high electrical conductivity. For the application, N-doped C is considered as one of the most promising supports to synthesis a serials of atomically dispersed metal single atoms,[95] leading to M_1-N-C electrocatalysts, including Co_1-N-C,[21a, 23a, 96] Fe_1-N-C,[97] Ni_1-N-C,[19d] Ru_1-N-C,[25] Pt_1-N-C,[22b] Pd_1-N-C,[98] and Cu_1-N-C[99] materials. These single atom catalysts have shown their multi-functional properties, which have been extensively used in ORR, OER, HER, CO oxidation, hydrogenation of quinoline, visible-light reduction of carbon dioxide, photocatalytic H_2 Evolution, hydrogenative coupling of nitroarenes, oxidation of alcohols, Zn-air battery. Li's group has developed a general method for the preparation of single atoms via N coordination with the assistance of ZIF-8 and ZIF-67. Impressively, the ZIF-derived Co_1-N-C and Fe_1-N-C could exhibit superior ORR performance than commercial Pt/C catalysts in alkaline electrolyte, which achieve half-wave potentials of 0.881 and 0.900 V, respectively (Figure 14a and b). The high activity is ascribed to that the single Co and Fe atoms could transport electrons to absorbed OH species.[23a, 97a] In addition, Pt_1 on N-doped carbon black can be utilized as a high-active catalyst for four-electron ORR in an acidic media, in which the Pt single atoms are bonded with single pyridinic N atoms to form Pt_1-N_1 active sites. This active sites surprisingly cleave O_2 on one Pt atom *via* $4e^-$ transfer (Figure 14c).[21c] Moreover, a catalyst consisted of Pt_1 on N-doped graphene nanosheets also outperform the Pt NP and commercial Pt/C catalysts for HER in acidic media. The superior activity of Pt_1 was proven to result from the partially unoccupied Pt *5d*-like orbitals, which are favourable to absorb H and resulted H_2 (Figure 14d).[100] g-C_3N_4 is accordingly regarded as a promising candidate owing to its high stability, excellent visible-light absorption, and capability to bind noble metal centres through N donor atoms. Pt_1 on g-C_3N_4 (Pt_1/g-C_3N_4) exhibited 50 times higher photocatalytic HER activity than g-C_3N_4 and eight

times higher TOF per atom than Pt NP/g-C_3N_4 (Figure 14e). The application of supported single atoms has recently extended to photocatalytic conversions. Ideally, the supports are supposed to absorb solar light and also stabilize the anchored single atoms. It is ascribed to that the Pt single atoms could change the surface trap states of g-C_3N_4, thereby enhancing photo-generated electron–hole separation.[22b] Additionally, g-C_3N_4 support is believed to deliver H atoms to Pt_1 and Pd_1 single atoms via DFT calculation, which render them high active catalysts for CO_2 photoreduction.[98] Due to the unknown nature of the active sites, the N donor atoms vary from two to six, in which the materials typically have metals bound to four N atoms. Beyond the intrinsic activity of M_1-N_x active sites, the pore structure and electrical conductivity of the carbon matrixes could affect mass and electron transport of the catalysts, leading to case-by-case performance. Our previous study shown the less number of N atoms adjacent to Pt in the four-coordinated structure corresponds to the smaller overpotential in ORR (Figure 14f).[101]

4.1.3 M_1-metal alloy

In general, the surface metal-matal bond created large perturbations in the electronic, chemical, and catalytic properties of metal center.[102] Especially, it is believed that the dissimilar metal atoms can produce charge transfer, which is the key role in modifying the chemical properties of the metal matrix layers and determining the cohesive energy, comparing with the bulk alloys. Since the isolated metal atom shown a tendency to fully use of the large number of valence orbitals, controlling the donation and acceptance of electrons, the single atom would provide a useful way to tune a metal catalyst's electronic structure and thus enhance its performance via its isolating activation ad desorption steps.[103] Also, the Cu particles have been extensively investigated as supports in both experimentally and theoretically. Scientists found that the d band of 0.5eV for the single metal Cu (solute atom) doped on Ag (matrix atom) became several times narrower than those of 2.5eV for bulk material Cu (Figure 15a). The computational calculation and photoemission spectroscopy measurements revealed that the solute's d states

resemble those of a free atom, whereby the d-electron orbitals are nearly degenerated, showing a clear charge transfer (Figure 15b). Especially, when it is in dilute concentrations, the solute-solute bonding disappeared and exhibited a weak interaction with the electronic states of the matrix element due to the minimal energetic and spatial overlap between the solute and matrix atoms.[104] The atomic resolution of the Pd/Cu alloy on the upper terrace (inset) shows the isolated Pd atoms in the surface layer appearing as protrusions. They found that a single atom alloy, with individual Pd atoms in a Cu(111) surface, could show lower energy barrier for both hydrogen dissociation and subsequent desorption (Figure 15c). The facile hydrogen dissociation at Pd SAs and weak binding on Cu substrate synergistically result in high hydrogenation selectivity of styrene and acetylene in contrast to pure Cu or Pd metal alone.[27a] A PdCu SAA with trace amount of Pd (0.18 at. %) was reported to demonstrate high activity and selectivity for the hydrogenation of butadiene to butenes. By the same method, they also synthesized Cu-alloyed Pd single atoms supported on Al_2O_3 via the galvanic replacement method, which exhibited both high conversion and styrene selectivity for selective hydrogenation of phenylacetylene.[27c] More recently, Pei *et al.* successfully synthesized silica gel supported Cu-alloyed Pd SAA by a simple incipient wetness co-impregnation method. They found that this $PdCu/SiO_2$ exhibited a high selectivity of ~85% with 100 % complete acetylene elimination toward the semihydrogenation of acetylene. The IB-metal-alloyed Pd SACs were also systematically compared with Cu-alloyed Pd SAC, in which similar active sites and catalytic mechanisms were revealed for the three catalysts. The further DFT calculation results indicated that the distinct conversion and selectivity of Pd atoms in the IB metal alloys is ascribed to the electron transfer between the IB mentals and Pd.[27d] Similarly, it is reported that a trace amount of Ni was employed to atomically disperse on Cu particles forming NiCu alloy (NiCu SAA). In-situ diffused reflectance infrared Fourier transform spectroscopy (DRIFTS) was employed in this work and identified that the C-H activation is the rate-

determining step of the dehydrogenation reaction on all the copper catalysts. The presence of Ni single atoms shown unique catalytic activities in the selective non- oxidative ethanol dehydrogenation reaction, owing to the exceptional low C-H bond activation barrier achieved via the effects between Ni isolated atoms and Cu particles. Also, comparing with Cu/SiO_2 monometallic nanoparticles, the NiCu SAA facilitated the formation of acetaldehyde in a low temperature of 150 ℃, showing a direct evidence of the key role in C-H bond scission of ethanol dehydrogenation (Figure 15d).[27e] The Pt_1 single atom on Cu particles illustrate a similar high efficient activation of C-H bond. The $Pt_{0.03}Cu$ SAC and $Pt_{0.01}Cu$ SAC start to convert butane (C_4H_{10}) to deuterated butane (C_4H_9D) at ~250 °C while the pure Cu-NP is showing activity at temperatures above 500 °C. Also, the reactivity of $Pt_{0.01}Cu$ SAC can be stable for 52 h at 400 °C with coke-resistance, which means the single atom Pt highly reduces the poisonous effect from CO_2. The PtCu SAC exhibits intermediate barrier compared with the pure Cu and pure Pt, which explains that single atom Pt readily activate C-H bonds in adsorbed CH_3*, resisting coke formation. However, the strong binding of CH_x intermediates to the Pt(111) surface compared to Cu(111) cause coke forming on Pt (Figure 15e).[105] As a natural expansion of the SAA concept, Liu *et al.* address the issue of CO poisoning of Pt catalysts via using Pt single atom based alloy in which the Pt atoms are embedded in a host metal surface, such as Cu. The situation for isolated Pt atoms is likely very different with traditional bimetallic alloys, where ensemble effects have been shown to increase the CO binding strength at extended catalytic metal sites.[106]

4.1.4 M_1-other supports

Besides metal oxides, carbon-based materials, and metal alloy, there are other supports, which was also used as host materials, including metal sulphides, metal nitrides, and metal carbides. The different host materials provide varieties of local structures due to the change of thickness, phases, and strains. The alternation of the local environment of foreign atoms arise a series of

differences of the surface engineering, such as orbital exchange-coupling interaction, the electronic band gap, electron density, and adsorption energy.

This support effects can be emphasized by Yang *et al*. via anchoring single-atom Pt catalyst on two different supports of titanium carbide and titanium nitride toward ORR reaction. Experimentally, they and coworkers synthesized two platforms: TiC and TiN to anchor Pt single atoms, showing there were big difference in catalytic activity, selectivity and stability. The oxygen reduction current density of Pt_1/TiC was almost two times larger than that of Pt_1/TiN at all potential ranges. Also, the Pt_1/TiC catalyst showed higher activity and higher selectivity toward H_2O_2 than Pt_1/TiN. However, unlike the single-atom catalysts, Pt particles on TiC and TiN demonstrated a similar performance of ORR activity and selectivity toward H_2O_2, indicating that support effects had essential role on their unique catalytic ability and selectivity. The DFT calculation was performed in this work to further explain the reason how the atomic dispersed active sites synergistically affect the ORR chemistry combining with support. Pt_1/TiN facilitate the dissociation of OOH* to O and OH rather than to the molecularly intact state, indicating the oxygen-oxygen bond would be dissociated more easily on Pt_1/TiN than on Pt_1/TiC. The energy profile shown that Pt/TiN (100) requires two successive energy uphill steps (052 and 0.94 eV) to produce H_2O_2, opposite to the case for Pt/TiC (100) at the same reaction coordinates. The adsorption energies of oxygen species on TiC and TiN predicted that there is less formation of H_2O_2 on than that on Pt/TiC, resulting in differences on activity and selectivity. The obtained Pt_1/TiC showed higher activity, stability, and selectivity for electrochemical oxygen reduction to H_2O_2 production than Pt_1/TiN. DFT calculations indicated that oxygen species preserved as oxygen–oxygen bonds on the Pt_1/TiC catalyst, which leads to high selectivity toward H_2O_2 production. In contrast, Pt_1/TiN have strong affinity into oxygen species, possibly resulting in surface poisoning species. The work clearly confirms that the supports in SACs could actively participate in

the surface reaction but not just provide anchoring sites for single atoms.[18b] DFT calculations found that the catalytic activity of TiC is expected to be active and selective for CO_2 reduction to CH_4, while TiN is limited for this process due to strong oxygen affinity.[57] Also, the double transition metal MXene nanosheets $Mo_2TiC_2T_x$, and monolayer MoS_2 have been successfully used as support to anchor single atoms. The single Pt atoms was immobilized on Mo vacancies enhance the HER catalytic activity of MXene's catalytic activity, which is 40 times greater than the commercial platinum-on-carbon catalyst. Similarly, the single atom Co_1 was doped in the S vacancy forming Co-S-Mo interfacial site, which exhibited superior activity, selectivity and stability for the hydrodeoxygenation of 4-methylphenol to toluene.[17b] The single atom Co displays a superior activity of 7,772.5 ml s^{-1} mol_{Co}^{-1} in terms of activity expressed per mole, which is 89 times more active than that of the typically reported $CoMoS_x/Al_2O_3$ catalyst (87.3 ml s^{-1} mol_{Co}^{-1}) under comparable conditions.

4.2 Catalytic Stability

Catalytic stability of SACs is an important factor that often hinders the application of SACs. Due to their high surface-free energy and the low coordination number, SACs are prone to sinter/ripen with time and catalytic processes, agglomerating into their thermodynamically stable state, such as particles.[36c, 107]

Even though thermally stable SACs can be successfully synthesized on various supports, it is predictable that chemical or reaction stabilization of these surface single atoms remains to be a challenge due to the presence of oxidative or reducing reactants and high temperature under operating conditions. Reaction stability of SACs is of great importance to design more robust catalysts. For instance, Flytzani-Stephanopoulos's group introduced alkali ions (Na or K) on zeolites and mesoporous oxides, to stable the single-site cationic Au-$O(OH)_x$- species.[108] They also prepared single-atom-centric Pt sites stabilized by sodium through –O ligands, which are

active and stable in WGS reaction from ~120 to 400 °C.[109] Reactants, such as CO, NO, H_2, and O_2, were confirmed to affect or induce dramatically the sintering, disruption, and re-dispersion of supported metal particles and single atoms.[32b, 110] CO induced the coalescence of Pd adatoms supported on Fe_3O_4(001) surfaces at room temperature.[32b] For the Pt/Fe_3O_4 system, the CO-induced mobility leads to the agglomeration of Pt into subnanometer clusters, but on the other hand the presence of CO stabilizes the smallest clusters against decay.[110a] The strong interaction between the reactant and the metal adatom is essential for the synthesis of a catalyst with high thermal and chemical stability. Kyriakou *et al.* anchored single Pd atoms in the lattice matrix on Cu(111) surfaces to obtain an extremely stable SAC with strong Pd-Cu bonds.[27a] Zhang's group prepared a series of single-atom Co–N–C catalysts with single Co atoms strongly bonded with four pyridinic N atoms, which showed high stability for the chemoselective hydrogenation of nitroarenes and aerobic oxidative cross-coupling of primary and secondary alcohols.[111] As shown in Figure 16a, the single atom Co-N-C catalyst was derived from pyrolysis of Co-phenanthroline complexes on a mesporous carbon support, which was proposed to be Co_1 bonded with N within graphitic sheets. This catalyst showed high catalytic activity toward the target reactions with turnover frequency of 3.8 s^{-1}. Impressively, the Co single atoms in the Co-N-C structure are highly stable against sintering during pyrolysis (< 800 °C) and acid leaching.[111a] Tang's group developed Ag_1-hollandite manganese oxide (HMO) catalyst with excellent thermal and chemical stability by initially depositing Ag NPs on HMO surfaces, and then annealing the sample at 500 °C in air. As revealed by Figure 16b, the HRTEM images confirmed that single-atom Ag linear chains were successfully synthesized via a simple thermal process. Figure 16c illustrated several models of this sample viewed from different directions with atom arrangement on the (001) facet of Ag-HMO. Moreover, temperature-dependent in situ XRD recorded the formation of this single atom Ag chain from 50 to 380 °C, in which the diffraction intensity of Ag(111) gradually decreases along shifting

to lower Bragg angles and then totally disappears after 230 ºC. The hollandite crystal structure remains unchanged in the whole process. Thus, Ag atoms can diffuse into the HMO tunnels to form a Ag atom chain inside, which exposed the end atoms on the surfaces to achieve SAC (Figure 16d).[13, 112] This Ag_1-HMO catalyst possessed four strong Ag–O bonds and one Ag–Ag bond, thereby showing high thermal stability at a temperature as high as 500 °C. Even when part of Ag–O bonds were broken during reactions such as HCHO oxidation, strong Ag–Ag bond can be well maintained by the exposing single Ag atoms after high-temperature chemical reactions.[13]

4.3 Selectivity

Selectivity are crucial when one catalytic reaction can undergo more than one reaction pathways. Although the molecules intermediates could present two or more reacting groups, only one of them is expected to be transformed. Thus, a selective catalyst must "recognize" and preferentially interact with the desired chemical group, while avoiding the transformation of the others. Single atoms feature with the uniformly dispersed, strongly anchored, and typically electron-deficient nature, which determine the regulable selectivity via changing the mode and strength of the reactant, intermediate and/or product adsorption or by changing the reaction pathway.

The tuning of SACs has been to the benefit of many reactions, especially selective hydrogenation. The frequently used catalysts hydrogenations are noble metals. Facile dissociation of reactants and week binding of intermediates are key requirements for efficient and selective catalysis. Unfortunately, the highly active noble metals are not chemoselective, which is usually addressed by utilizing stoichiometric reducing agents, realizing high chemoselectivity in the expense of lowering catalytic activity. The heterogeneous catalysts with high chemoselecitivity and activity are highly desired. Based on the uniform geometry of single atoms and their good capability for H_2 dissociation,[27a] Zhang's group reported novel

FeO_x supported Pt single-atom and pseudo-single-atom structure as highly active and chemoselective catalyst on hydrogenation of functionalized nitroarenes. The strong metal-support interaction leads to significant electron transfer from the Pt atoms or ensembles to the FeO_x support. The presence of positively charged Pt centers, the absence of Pt-Pt metallic bonding and the reduced metal oxide surfaces are synthetically favourable to the absorption of nitro groups, which determines significantly improved performance.[9d] The selectivity of a nitro group into an amino group has been investigated by catalysing with various heterogeneous single atoms. The Pt_1/FeO_x shows outstanding activity and chemoselectivity with low Pt_1 loading ratio (0.08 wt. %),[9d] giving rise to a TOF of ~1500 h^{-1} and 99% selectivity to 3-aminostyrene from 3-nitrostyrene. The high chemoselectivity is due to the partially anionic O atoms of the $–NO_2$ group can strongly binds with the isolated cationic Pt centers. This favourable phenomenon is more effective when introducing alkali metal cations to Pt_1/FeO_x with high Pt loadings, leading to >20-fold mass activity with similarly high TOF values and chemoselectivities.[113] It should be pointed out that the support plays a critical role in tuning selectivity for hydrogenation of nitroarenes. On the other hand, Pd_1 exhibited high activity and selectivity for the selective hydrogenation of C≡C bonds, C=C bonds, and other unsaturated systems.[19c, 22a, 27a, 27c, 27d, 114] Interestingly, no matter what supports are, the Pd_1 without the Pd-Pd bonding always show superior performance, which is due to the multinuclear sites could strongly bind ethylene and promote the further hydrogenation to ethane. The product selectivity of hydrogenation of CO_2 is very sensitive to the size the active sites. The single atoms can easily release CO with relatively few H atoms present to further reduce CO; while NPs surface with many H atoms is favourable to the formation of CH_4. Despite of the size effect, the strong metal-support interaction (SMSI) could tune the chemical state of single atoms and thus have significant impact on the reaction selectivity. For instance, Kwark *et al.* demonstrated fundamentally different activity and selectivity via comparing Pd_1 and traditional 3D Pd cluster

on different supports for the reaction of CO_2 reduction. (Figure 17a). For instance, Pd_1,[74] Ru_1,[115] and Rh_1[116] are highly selective for the pathway of CO formation as part of the reverse WGS reaction. In contrast, the corresponding particles tend to induce CH_4 as the major product due to the size effect. These support effects can be emphasized by Yang *et al*. via anchoring single-atom Pt catalyst on two different supports of titanium carbide and titanium nitride toward ORR reaction (Figure 17b). Experimentally, they synthesized two platforms: TiC and TiN to anchor Pt single atoms, showing there were big difference in catalytic activity, selectivity and stability. The oxygen reduction current density of Pt_1/TiC was almost two times larger than that of Pt_1/TiN at all potential ranges. Also, the Pt_1/TiC catalyst showed higher activity and higher selectivity toward H_2O_2 than Pt_1/TiN. However, unlike the single-atom catalysts, Pt particles on TiC and TiN demonstrated a similar performance of ORR activity and selectivity toward H_2O_2, indicating that support effects had essential role on their unique catalytic ability and selectivity. The DFT calculation was performed in this work to further explain the reason how the atomic dispersed active sites synergistically affect the ORR chemistry combining with support. Pt_1/TiN facilitate the dissociation of OOH* to O and OH rather than to the molecularly intact state, indicating the oxygen-oxygen bond would be dissociated more easily on Pt_1/TiN than on Pt_1/TiC. The energy profile shown that Pt/TiN (100) requires two successive energy uphill steps (052 and 0.94 eV) to produce H_2O_2, opposite to the case for Pt/TiC (100) at the same reaction coordinates. The adsorption energies of oxygen species on TiC and TiN predicted that there is less formation of H_2O_2 on than that on Pt/TiC, resulting in differences on activity and selectivity. The obtained Pt_1/TiC showed higher activity, stability, and selectivity for electrochemical oxygen reduction to H_2O_2 production than Pt_1/TiN. DFT calculations indicated that oxygen species preserved as oxygen–oxygen bonds on the Pt_1/TiC catalyst, which leads to high selectivity toward H_2O_2 production. In contrast, Pt_1/TiN have strong affinity into oxygen species, possibly resulting in surface

poisoning species. The work clearly confirms that the supports in SACs could actively participate in the surface reaction but not just provide anchoring sites for single atoms.[18b] DFT calculations found that the catalytic activity of TiC is expected to be active and selective for CO_2 reduction to CH_4, while TiN is limited for this process due to strong oxygen affinity.[57]

Similarly, single atom catalysts are also conclusive to the electrochemical reduction of CO_2 over the HER due to the stronger surface absorption for CO_2 reduction intermediates than that of H atoms and being cationic of the active metal atoms.[24a, 57, 117] In particular, Ni_1-N-C catalysts are highly selective for the $2H^+/2e^-$ electro-reduction of CO_2 to CO with high Faradaic efficiency (> 90%).[24a, 117d] Figure 17c showed that the single-atom A-Ni-NSG (single nickel atoms dispersed on nitrogenated graphene with a sulphur precursor) electrode exhibits a maximum Faradaic efficiency (CO) of about 97% at around -0.5 V (versus RHE). Further reduction of CO to methane is completely suppressed because of the weak binding of CO to the single Ni atom site. Notably, the two single-Ni-atom catalysts maintain greater than 80% selectivity towards CO formation, even at very negative applied potentials, and this selectivity is almost independent of the proton concentration.[117d] Fe_1-N-C catalysts are active and selective toward the formation of CH_3CO_2H with selectivity of 61% and Faradaic efficiency of 97.4% (Figure 17d) at very low potential.[118] The selectivity of ORR reactions could be deliberately tuned from a $4e^-$ ($4H^+ + 4e^- + O_2 \rightarrow 2H_2O$) to a $2e^-$ ($2H^+ + 2e^- + O_2 \rightarrow H_2O_2$) pathway via taking advantage of single atoms. For instance, Pt_1-TiN,[18a] Pt_1-Hg,[119] and Pd_1-Hg-C[120] exhibit high selectivity of H_2O_2, which is due to the absence of metal-metal bonding. Thus, these SACs do not possess the reducing equivalents to reduce O_2 to H_2O, which generally requires at least two adjacent active metal sites. Also, Gu *et al.* has proposed that the interaction between Pt_1/Au_1 atoms and Zn (10-01) nanofacets leads to positively charged Pt_1 and Au_1

atoms, which could facilitate the adsorption of reaction intermediates during MSR and thus modify the reaction pathways.[11]

5. Conclusions and perspectives

SACs have gained increasing interest due to very different catalytic behaviours from that of nanoparticles and bulk counterparts. In this review, the support effects associated to the atomic-local environments of single atoms has been emphasized both on SACs fabrication and catalytic behaviours. Moreover, combined with the experimental results, the theoretical calculations on electronic configurations of SACs can be used to empirically screen interaction strengths between metal-support pairs, thus aiding the design and synthesis of single-atom catalysts on various supports. The unique electronic structures of different SACs require suitable atomic-local environments, with designed coordination atoms anchoring in appropriate supports, to reduce the energy barriers and achieve optimal catalytic properties. On the other hand, the support surface through strong metal-support interactions leads to the polarization of these heteroatomic bonds and substantial charge transfer from the active metal to the support. These electron-deficient single metal sites are responsible for distinctive catalytic properties. The supports definitely play an essential role to determine those key catalytic characters and showing how to rationally design an efficient support-SACs structure to enhance the activity and selectivity in each special reaction.

M_1-metal oxide. A variety of metal oxides based supports have been explored, on which diverse single metal sites can be successfully anchored on these substrates without agglomeration. For instance, the metal oxides, such as inert metal oxides (Al_2O_3, MgO, and SiO_2) and active metal oxides (ZnO, Fe_2O_3, WO_x, CeO_2, and TiO_2), can modify with lone electron pairs oxygen defects, such as oxygen vacancies, the ethylene glycolate and hydroxyl groups, to define metal species. The coordination between supports and metal species leads to strong interaction, inhibiting the aggregating of anchored metal sites. The theoretical

calculation revealed the single atoms interacts with O atom on both inert and active metal oxides. On the one hand, significant charge transfer takes place between single atom and the surface, which results in the charge redistribution from the neighbouring oxygen and metal atoms when active metal oxide is used as support. Also, charge accumulation was observed in a metal-metal hybrid orbital. On the other hand, for the irreducible MgO (100), it is unable to readily accept electron density from a metal adatom but instead reduces the metal adatoms. The metal-support interactions are localized onto one surface oxygen via transferring electron density from the support to the adsorbed single atoms. It is noted that when the single atom is doped on the inert substrates, such as Al_2O_3, and MgO, the as prepared catalysts are commonly utilized in oxidized reaction, such as CO oxidation, while active metal oxide based catalysts can be used as in both oxidized reaction and reduced reaction, such as ORR, HER, and CRR. Furthermore, it shows that active substrates have the higher active and selectivity compared the inert one. It can conclude that, besides the M_1-O-Metal interaction, the M_1-reducible metal bonds is of significance in increase the activity of catalysts and exploring more applications.

M_1-N_x-C_y. The nitrogen-doped carbon is the most commonly used carbon based supports to stabilize single atoms. Fortunately, nitrogen doped carbon supports have a plenty of carbonaceous sources, meaning that the metal species can be coordinated via many ways, such as nitrogen sources-sintering carbon, graphitic carbon nitride, metal organic frameworks. The nitrogen sources-sintering carbon, such as NH_3, has been considering that the formed pyridinic (P)-N has the strong anchoring sites for single metal atoms due to the modified interfacial interaction. This suggests that the metal atoms can be selectively trapped strongly by C-N site and thus stabilize the dispersion of single atoms on carbon surface, confirming the vital role of support properties on the formation of single atoms. The pyrolysis process of the nitrogen contained organic structure can strongly stabilize varieties of metal species, forming metal-N_x-C_y structure. Although many previous reports have been considered the nitrogen on the N-

doped carbon as the key role, it is better to define the nitrogen as 'nitrogen-contained group'. For example, the MOF derived nitrogen doped carbon has never been directly successfully used and doped with single atom, but MOF structures have been confirmed many times that they can used as substrates to anchor single atoms. The local structure M_1-N_x-C_y has been intensively applied in various catalytic reaction, including ORR, HER, OER, CRR, hydrogenation, and acetylene hydrochlorination. Notably, it is vital to tune the M_1 and N in the local structure M_1-N_x-C_y. It is been theoretically confirmed that tuning different single metal atoms can decrease the energy barrier and improve their catalytic activity in both CRR and HER. The N ratio strongly affects the conductivity of the substrates so that affects their ability in charge-transfer. Our previous work revealed the activity of ORR of Pt-N-C would increase when the ratio of N species decreased.[101]

M_1-metal. Compared with carbon-based supports, the formation of single atoms on metal-based surface exhibits different geometric and electronic structures, that is, only a trace amount of heterogeneous metal species can be doped to form bimetallic catalysts. SAAs comprise by alloying catalytically active elements like Pt, Pd, and Ni with more insert support metals via the simple wet-chemistry methods. Both model studies and experimental results confirm the distinct advantages of SAAs for industrial applications. (1) The typical fabrication methods for SAAs are easy to scale up for real applications. (2) The well-defined nature of the active sites in SAAs enable them easy to understand and realize rational design of SAAs via modelling theory. (3) The SAAs could tackle important challenges in industrial processes, such as CO poisoning, tolerance to coking, and high activity coupled with extraordinary selectivity. (4) The most common application of SAAs is based on C-H activation, such as PtCu SAAs towards butane hydrogenation,[121] PtNi for hydrogenation from aqueous ammonia-borane,[122] NiCu for ethanol dehydrogenation,[123] and PdCu for phenylacetylene hydrogenation,[27b] which can achieve both effective dissociation of reactants and weak binding of intermediates, leading to

high selectivity, stability, and resistance to poisoning. Beyond that, the SAAs can be used in other fields as well, such as electrocatalytic hydrogen evolution,[54, 124] photocatalytic conversion,[125] and hydrogen storage.[126]

M_1-other supports. Similarly, carbon-vacancy, sulphur-vacancy, titanium-vacancy, and the nitrogen-vacancy in supports, such as MoS_2, TiC, TiN, and MXene, were also found to show strong interactions with metal ions forming single atom sites. These specific substrates can develop particular local structures, which show special activity in catalytic reactions. For instance, the metal atoms, such as V, Ti, Fe, Mn, Cr, etc., could substitute the Mo atoms in the MoS_2 matrix, remaining in the middle to bond with six S atoms, which can be anticipated to possess low activity due to their weak binding ability with H. The other metal atoms, such as Pt, Ag, Pd, Co, Ni, etc., however, are prone to shift toward one side and bond with only four S atoms but leave other two S atoms unsaturated, leading to distinctly high adsorption behaviours of H atoms on the two unsaturated S atoms and thereby high HER activity. In sum, the successful exploration of single atoms with more new substrates could lead a promising direction of diverse atomic materials toward various catalytic reactions.

For future research, it is essential to develop more SACs with high thermal/chemical stability and excellent catalytic performance. Notably, the current loading ratio of SACs is relatively low. In order to enhance the catalytic performance of various SACs, it is urgent to explore various strategies to achieve high loading ratio, such as developing synthesis methods and modifying the surface of supports. Manipulating strong interactions between SACs and supports with abundant anchoring sites would hold great promise for this target. Furthermore, it is also worthwhile to better understand the impact of single-atom loading amounts on catalytic activity. The increased loading ratio of single atoms inevitably would occupy more sites within the supports, which may affect the electronic structure of SACs.[127] As a result,

there could be thresholds of single-atom loading ratios in SACs towards the optimal activity towards different catalytic reactions.

On the other hand, the understanding of the catalytic mechanism and performance based on the interactions between SACs and supports should be further deepened at the atomic scale by employing SACs as model systems with the aid of theoretical calculation and in situ characterization. Moreover, we believe the synergistic effect of different types of SACs is very critical in optimizing catalytic performance for diverse reactions. It opens a new avenue for structure design and material synthesis, in which a series of binary/ternary/multi-phase SACs are waiting to be explored. The further study on optimal doping levels and ratios is also significant and meaningful. Therefore, more efforts on the applications of SACs could be extended to a wide range of useful catalytic reactions for energy generation, water purification, gas emission control, and production of chemicals. Research along this SACs direction is expected to be very interesting and fruitful.

Acknowledgements

This work is financially supported by the Australian Research Council (ARC) (LP120200432, DE170100928 and DP140104062). We also thank Dr. Tania Silver for critical reading of the manuscript.

Received: ((will be filled in by the editorial staff))

Revised: ((will be filled in by the editorial staff))

Published online: ((will be filled in by the editorial staff))

References

[1] J. S. Kim, B. Kim, H. Kim, K. Kang, *Adv. Energy Mater.* **2018**, 8.

[2] B. Qiao, A. Wang, X. Yang, L. F. Allard, Z. Jiang, Y. Cui, J. Liu, J. Li, T. Zhang, *Nat. Chem.* **2011**, 3, 634.

[3] J. Liu, *ACS Catal.* **2016**, 7, 34.

[4] a) S. Tauster, S. Fung, R. L. Garten, *J. Am. Chem. Soc.* **1978**, 100, 170; b) S. J. Tauster, *Acc. Chem. Res.* **1987**, 20, 389.

[5] V. E. Henrich, P. A. Cox, *The surface science of metal oxides*, Cambridge University Press, **1996**.

[6] a) X.-F. Yang, A. Wang, B. Qiao, J. Li, J. Liu, T. Zhang, *Acc. Chem. Res.* **2013**, 46, 1740; b) S. Mitchell, E. Vorobyeva, J. Pérez-Ramírez, *Angew. Chem. Int. Ed.Angew. Chem. Int. Ed.* **2018**, 57, 15316; c) L. Liu, A. Corma, *Chem. Rev.* **2018**, 118, 4981; d) A. Wang, J. Li, T. Zhang, *Nat. Rev. Chem.* **2018**, 2, 65; e) J. Zhang, C. Liu, B. Zhang, *Small Methods* **2019**, 1800481.

[7] a) B. Qiao, J. Liu, Y.-G. Wang, Q. Lin, X. Liu, A. Wang, J. Li, T. Zhang, J. Liu, *ACS Catal.* **2015**, 5, 6249; b) F. Dvořák, M. F. Camellone, A. Tovt, N.-D. Tran, F. R. Negreiros, M. Vorokhta, T. Skála, I. Matolínová, J. Mysliveček, V. Matolín, *Nat. Commun.* **2016**, 7, 10801; c) J. Jones, H. Xiong, A. T. DeLaRiva, E. J. Peterson, H. Pham, S. R. Challa, G. Qi, S. Oh, M. H. Wiebenga, X. I. P. Hernández, *Science* **2016**, 353, 150.

[8] a) M. Moses-DeBusk, M. Yoon, L. F. Allard, D. R. Mullins, Z. Wu, X. Yang, G. Veith, G. M. Stocks, C. K. Narula, *J. Ame. Chem. Soc.* **2013**, 135, 12634; b) Z. Zhang, Y. Zhu, H. Asakura, B. Zhang, J. Zhang, M. Zhou, Y. Han, T. Tanaka, A. Wang, T. Zhang, *Nat. Commun.* **2017**, 8, 16100; c) X. Cui, K. Junge, X. Dai, C. Kreyenschulte, M.-M. Pohl, S. Wohlrab, F. Shi, A. Brückner, M. Beller, *ACS Cent. Sci.* **2017**, 3, 580; d) C. K. Narula, L. F. Allard, G. Stocks, M. Moses-DeBusk, *Sci. Rep.* **2014**, 4, 7238; e) Z.-Y. Li, Z. Yuan, X.-N. Li, Y.-X. Zhao, S.-G. He, *J. Ame. Chem. Soc.* **2014**, 136, 14307.

[9] a) J. Lin, A. Wang, B. Qiao, X. Liu, X. Yang, X. Wang, J. Liang, J. Li, J. Liu, T. Zhang, *J. Ame. Chem. Soc.* **2013**, 135, 15314; b) B. Qiao, J.-X. Liang, A. Wang, C.-Q. Xu, J. Li, T. Zhang, J. J. Liu, *Nano Res.* **2015**, 8, 2913; c) J. Lin, B. Qiao, N. Li, L. Li, X. Sun, J. Liu, X. Wang, T. Zhang, *Chem. Commun.* **2015**, 51, 7911; d) H. Wei, X. Liu, A. Wang, L. Zhang, B. Qiao, X. Yang, Y. Huang, S. Miao, J. Liu, T. Zhang, *Nat. Commun.* **2014**, 5, ncomms6634.

[10] a) P. Liu, Y. Zhao, R. Qin, S. Mo, G. Chen, L. Gu, D. M. Chevrier, P. Zhang, Q. Guo, D. Zang, *Science* **2016**, 352, 797; b) L. DeRita, S. Dai, K. Lopez-Zepeda, N. Pham, G. W. Graham, X. Pan, P. Christopher, *J. Ame. Chem. Soc.* **2017**, 139, 14150.

[11] X.-K. Gu, B. Qiao, C.-Q. Huang, W.-C. Ding, K. Sun, E. Zhan, T. Zhang, J. Liu, W.-X. Li, *ACS Catal.* **2014**, 4, 3886.

[12] C. Wang, G. Garbarino, L. F. Allard, F. Wilson, G. Busca, M. Flytzani-Stephanopoulos, *ACS Catal.* **2015**, 6, 210.

[13] Z. Huang, X. Gu, Q. Cao, P. Hu, J. Hao, J. Li, X. Tang, *Angew. Chem. Int. Ed.* **2012**, 124, 4274.

[14] K. Ding, A. Gulec, A. M. Johnson, N. M. Schweitzer, G. D. Stucky, L. D. Marks, P. C. Stair, *Science* **2015**, 350, 189.

[15] L. Wang, H. Li, W. Zhang, X. Zhao, J. Qiu, A. Li, X. Zheng, Z. Hu, R. Si, J. Zeng, *Angew. Chem. Int. Ed.Angew. Chem. Int. Ed.* **2017**, 56, 4712.

[16] J. Wang, X. Zhao, N. Lei, L. Li, L. Zhang, S. Xu, S. Miao, X. Pan, A. Wang, T. Zhang, *ChemSusChem* **2016**, 9, 784.

[17] a) J. Deng, H. Li, J. Xiao, Y. Tu, D. Deng, H. Yang, H. Tian, J. Li, P. Ren, X. Bao, Energy Environ. Sci. **2015**, 8, 1594; b) G. Liu, A. W. Robertson, M. M.-J. Li, W. C.

Kuo, M. T. Darby, M. H. Muhieddine, Y.-C. Lin, K. Suenaga, M. Stamatakis, J. H. Warner, *Nat. Chem.* **2017**, 9, 810.

[18] a) S. Yang, J. Kim, Y. J. Tak, A. Soon, H. Lee, *Angew. Chem. Int. Ed.Angew. Chem. Int. Ed.* **2016**, 55, 2058; b) S. Yang, Y. J. Tak, J. Kim, A. Soon, H. Lee, *ACS Catal.***2017**, 7, 1301.

[19] a) H. Wang, Q. Wang, Y. Cheng, K. Li, Y. Yao, Q. Zhang, C. Dong, P. Wang, U. Schwingenschlögl, W. Yang, *Nano Lett.* **2011**, 12, 141; b) S. Sun, G. Zhang, N. Gauquelin, N. Chen, J. Zhou, S. Yang, W. Chen, X. Meng, D. Geng, M. N. Banis, *Sci. Rep.* **2013**, 3, 1775; c) H. Yan, H. Cheng, H. Yi, Y. Lin, T. Yao, C. Wang, J. Li, S. Wei, J. Lu, *J. Ame. Chem. Soc.* **2015**, 137, 10484; d) H. J. Qiu, Y. Ito, W. Cong, Y. Tan, P. Liu, A. Hirata, T. Fujita, Z. Tang, M. Chen, *Angew. Chem. Int. Ed.Angew. Chem. Int. Ed.* **2015**, 54, 14031.

[20] a) X. Zhang, J. Guo, P. Guan, C. Liu, H. Huang, F. Xue, X. Dong, S. J. Pennycook, M. F. Chisholm, *Nat. Commun.* **2013**, 4, 1924; b) G. Malta, S. A. Kondrat, S. J. Freakley, C. J. Davies, L. Lu, S. Dawson, A. Thetford, E. K. Gibson, D. J. Morgan, W. Jones, *Science* **2017**, 355, 1399.

[21] a) H. Fei, J. Dong, M. J. Arellano-Jiménez, G. Ye, N. D. Kim, E. L. Samuel, Z. Peng, Z. Zhu, F. Qin, J. Bao, *Nat. Commun.* **2015**, 6, 8668; b) C. Zhang, J. Sha, H. Fei, M. Liu, S. Yazdi, J. Zhang, Q. Zhong, X. Zou, N. Zhao, H. Yu, *ACS Nano* **2017**, 11, 6930; c) J. Liu, M. Jiao, L. Lu, H. M. Barkholtz, Y. Li, Y. Wang, L. Jiang, Z. Wu, D.-j. Liu, L. Zhuang, *Nat. Commun.* **2017**, 8, 15938.

[22] a) G. Vilé, D. Albani, M. Nachtegaal, Z. Chen, D. Dontsova, M. Antonietti, N. López, J. Pérez-Ramírez, *Angew. Chem. Int. Ed.* **2015**, 54, 11265; b) X. Li, W. Bi, L. Zhang, S. Tao, W. Chu, Q. Zhang, Y. Luo, C. Wu, Y. Xie, *Adv. Mater.* **2016**, 28, 2427; c) Y. Zheng, Y. Jiao, Y. Zhu, Q. Cai, A. Vasileff, L. H. Li, Y. Han, Y. Chen, S.-Z. Qiao, *J. Ame. Chem. Soc.* **2017**, 139, 3336.

[23] a) P. Yin, T. Yao, Y. Wu, L. Zheng, Y. Lin, W. Liu, H. Ju, J. Zhu, X. Hong, Z. Deng, *Angew. Chem. Int. Ed.* **2016**, 55, 10800; b) L. Tao, C.-Y. Lin, S. Dou, S. Feng, D. Chen, D. Liu, J. Huo, Z. Xia, S. Wang, *Nano Energy* **2017**, 41, 417.

[24] a) C. Zhao, X. Dai, T. Yao, W. Chen, X. Wang, J. Wang, J. Yang, S. Wei, Y. Wu, Y. Li, *J. Ame. Chem. Soc.* **2017**, 139, 8078; b) Y. Chen, S. Ji, Y. Wang, J. Dong, W. Chen, Z. Li, R. Shen, L. Zheng, Z. Zhuang, D. Wang, *Angew. Chem. Int. Ed.* **2017**, 56, 6937.

[25] X. Wang, W. Chen, L. Zhang, T. Yao, W. Liu, Y. Lin, H. Ju, J. Dong, L. Zheng, W. Yan, *J. Ame. Chem. Soc.* **2017**, 139, 9419.

[26] H. Zhang, S. Hwang, M. Wang, Z. Feng, S. Karakalos, L. Luo, Z. Qiao, X. Xie, C. Wang, D. Su, *J. Ame. Chem. Soc.* **2017**, 139, 14143.

[27] a) G. Kyriakou, M. B. Boucher, A. D. Jewell, E. A. Lewis, T. J. Lawton, A. E. Baber, H. L. Tierney, M. Flytzani-Stephanopoulos, E. C. H. Sykes, *Science* **2012**, 335, 1209; b) M. B. Boucher, B. Zugic, G. Cladaras, J. Kammert, M. D. Marcinkowski, T. J. Lawton, E. C. H. Sykes, M. Flytzani-Stephanopoulos, Phys. Chem. Chem. Phys. **2013**, 15, 12187; c) F. R. Lucci, J. Liu, M. D. Marcinkowski, M. Yang, L. F. Allard, M. Flytzani-Stephanopoulos, E. C. H. Sykes, *Nat. Commun.* **2015**, 6, 8550; d) G. X. Pei, X. Y. Liu, X. Yang, L. Zhang, A. Wang, L. Li, H. Wang, X. Wang, T. Zhang, *ACS Catal.* **2017**, 7, 1491; e) J. Shan, N. Janvelyan, H. Li, J. Liu, T. M. Egle, J. Ye, M. M. Biener, J. Biener, C. M. Friend, M. Flytzani-Stephanopoulos, *Appl. Cataly. B: Environ.* **2017**, 205, 541.

[28] J. Zhang, J. Liu, L. Xi, Y. Yu, N. Chen, S. Sun, W. Wang, K. M. Lange, B. Zhang, *J. Ame. Chem. Soc.* **2018**, 140, 3876.

[29] F. Z. Song, Q. L. Zhu, X. Yang, W. W. Zhan, P. Pachfule, N. Tsumori, Q. Xu, *Adv. Energy Mater.* **2018**, 8, 1701416.

[30] a) A. Bruix, J. A. Rodriguez, P. J. Ramírez, S. D. Senanayake, J. Evans, J. B. Park, D. Stacchiola, P. Liu, J. Hrbek, F. Illas, *J. Ame. Chem. Soc.* **2012**, 134, 8968; b) Q. Fu, H. Saltsburg, M. Flytzani-Stephanopoulos, *Science* **2003**, 301, 935.

[31] a) Z. Novotný, G. Argentero, Z. Wang, M. Schmid, U. Diebold, G. S. Parkinson, *Phys. Rev. Lett.* **2012**, 108, 216103; b) R. Bliem, E. McDermott, P. Ferstl, M. Setvin, O. Gamba, J. Pavelec, M. Schneider, M. Schmid, U. Diebold, P. Blaha, *Science* **2014**, 346, 1215; c) R. Bliem, R. Kosak, L. Perneczky, Z. Novotny, O. Gamba, D. Fobes, Z. Mao, M. Schmid, P. Blaha, U. Diebold, G. S. Parkinson, *ACS Nano* **2014**, 8, 7531.

[32] a) Z. Novotny, N. Mulakaluri, Z. Edes, M. Schmid, R. Pentcheva, U. Diebold, G. S. Parkinson, *Phys. Rev. B* **2013**, 87, 195410; b) G. S. Parkinson, Z. Novotny, G. Argentero, M. Schmid, J. Pavelec, R. Kosak, P. Blaha, U. Diebold, *Nat. Mater.***2013**, 12, 724; c) R. Bliem, R. Kosak, L. Perneczky, Z. Novotny, O. Gamba, D. Fobes, Z. Mao, M. Schmid, P. Blaha, U. Diebold, *ACS Nano* **2014**, 8, 7531.

[33] Y. Lou, J. Liu, *Ind. Eng. Chem. Res.* **2017**, 56, 6916.

[34] J. Guzman, B. C. Gates, *J. Cataly.***2004**, 226, 111.

[35] M. Yang, L. F. Allard, M. Flytzani-Stephanopoulos, *J. Ame. Chem. Soc.* **2013**, 135, 3768.

[36] a) M. Chen, D. Goodman, *Science* **2004**, 306, 252; b) D. Matthey, J. Wang, S. Wendt, J. Matthiesen, R. Schaub, E. Lægsgaard, B. Hammer, F. Besenbacher, *Science* **2007**, 315, 1692; c) J. H. Kwak, J. Hu, D. Mei, C.-W. Yi, D. H. Kim, C. H. Peden, L. F. Allard, J. Szanyi, *Science* **2009**, 325, 1670.

[37] A. Bruix, Y. Lykhach, I. Matolínová, A. Neitzel, T. Skála, N. Tsud, M. Vorokhta, V. Stetsovych, K. Ševčíková, J. Mysliveček, *Angew. Chem. Int. Ed.Angew. Chem. Int. Ed.* **2014**, 53, 10525.

[38] M. M. Branda, R. M. Ferullo, M. Causà, F. Illas, *The Journal of Physical Chemistry C* **2011**, 115, 3716.

[39] Y.-F. Yu-Yao, J. Kummer, *J. Cataly.* **1987**, 106, 307.

[40] J.-C. Liu, Y.-G. Wang, J. Li, *J. Ame. Chem. Soc.* **2017**, 139, 6190.

[41] F. Boccuzzi, A. Chiorino, M. Manzoli, D. Andreeva, T. Tabakova, *J. Cataly.* **1999**, 188, 176.

[42] J.-X. Liang, J. Lin, X.-F. Yang, A.-Q. Wang, B.-T. Qiao, J. Liu, T. Zhang, J. Li, *J. Phys. Chem. C* **2014**, 118, 21945.

[43] X.-N. Li, Z. Yuan, S.-G. He, *J. Ame. Chem. Soc.* **2014**, 136, 3617.

[44] a) A. S. Hoffman, L. M. Debefve, S. Zhang, J. E. Perez-Aguilar, E. T. Conley, K. R. Justl, I. Arslan, D. A. Dixon, B. C. Gates, *ACS Catal.* **2018**, 8, 3489; b) Z. Zuo, S. Liu, Z. Wang, C. Liu, W. Huang, J. Huang, P. Liu, *ACS Catal.* **2018**, 8, 9821.

[45] K.-i. Otake, Y. Cui, C. T. Buru, Z. Li, J. T. Hupp, O. K. Farha, *J. Ame. Chem. Soc.* **2018**, 140, 8652.

[46] S. Ulrich, N. Nilius, H.-J. Freund, U. Martinez, L. Giordano, G. Pacchioni, *Phys. Rev. Lett.* **2009**, 102, 016102.

[47] C. Lee, X. Wei, J. W. Kysar, J. Hone, *Science* **2008**, 321, 385.

[48] C. Zhang, S. Yang, J. Wu, M. Liu, S. Yazdi, M. Ren, J. Sha, J. Zhong, K. Nie, S. Jalilov Almaz, Z. Li, H. Li, B. I. Yakobson, Q. Wu, E. Ringe, H. Xu, M. Ajayan Pulickel, J. M. Tour *Adv. Energy Mater.* **2018**, 8, 1703487.

[49] M. Zhang, Y.-G. Wang, W. Chen, J. Dong, L. Zheng, J. Luo, J. Wan, S. Tian, W.-C. Cheong, D. Wang, *J. Ame. Chem. Soc.* **2017**, 139, 10976.

[50] Y. Zheng, S.-Z. Qiao, *Nat. Sci. Rev.***2018**.

[51] X. Li, X. Huang, S. Xi, S. Miao, J. Ding, W. Cai, S. Liu, X. Yang, H. Yang, J. Gao, J. Wang, Y. Huang, T. Zhang, B. Liu, *J. Ame. Chem. Soc.* **2018**, 140, 12469.

[52] a) Y. Zheng, Y. Jiao, Y. Zhu, L. H. Li, Y. Han, Y. Chen, A. Du, M. Jaroniec, S. Z. Qiao, *Nat. Commun.* **2014**, 5, 3783; b) G. Gao, Y. Jiao, F. Ma, Y. Jiao, E. Waclawik, A. Du, *J. Cataly.* **2015**, 332, 149; c) J. Liu, Y. Liu, N. Liu, Y. Han, X. Zhang, H. Huang, Y. Lifshitz, S.-T. Lee, J. Zhong, Z. Kang, *Science* **2015**, 347, 970.

[53] B. Zhang, H. Asakura, J. Zhang, J. Zhang, S. De, N. Yan, *Angew. Chem. Int. Ed.Angew. Chem. Int. Ed.* **2016**, 55, 8319.

[54] J. Kim, C. W. Roh, S. K. Sahoo, S. Yang, J. Bae, J. W. Han, H. Lee, *Adv. Energy Mater.* **2018**, 8, 1701476.

[55] P. N. Duchesne, Z. Li, C. P. Deming, V. Fung, X. Zhao, J. Yuan, T. Regier, A. Aldalbahi, Z. Almarhoon, S. Chen, *Nat. Mater.***2018**, 17, 1033.

[56] Y. J. Tak, W. Jang, N. A. Richter, A. Soon, Phys. Chem. Chem. Phys. **2015**, 17, 9680.

[57] S. Back, Y. Jung, *ACS Energy Lett.***2017**, 2, 969.

[58] a) C. T. Campbell, S. C. Parker, D. E. Starr, *Science* **2002**, 298, 811; b) S. C. Parker, C. T. Campbell, *Phys. Rev. B* **2007**, 75, 035430.

[59] J. A. Farmer, C. T. Campbell, *Science* **2010**, 329, 933.

[60] K. T. Rim, D. Eom, L. Liu, E. Stolyarova, J. M. Raitano, S.-W. Chan, M. Flytzani-Stephanopoulos, G. W. Flynn, *J. Phys. Chem. C* **2009**, 113, 10198.

[61] F. Li, Y. Li, X. C. Zeng, Z. Chen, *ACS Catal.* **2014**, 5, 544.

[62] Y. Zhu, T. Cao, C. Cao, J. Luo, W. Chen, L. Zheng, J. Dong, J. Zhang, Y. Han, Z. Li, *ACS Catal.* **2018**, 8, 10004.

[63] J. Casanovas, J. M. Ricart, J. Rubio, F. Illas, J. M. Jiménez-Mateos, *J. Ame. Chem. Soc.* **1996**, 118, 8071.

[64] E. Fako, Z. Łodziana, N. López, *Cataly. Sci. Technol.* **2017**, 7, 4285.

[65] N. J. O'Connor, A. Jonayat, M. J. Janik, T. P. Senftle, *Nat. Cataly.* **2018**, 1, 531.

[66] a) T. Yang, R. Fukuda, S. Hosokawa, T. Tanaka, S. Sakaki, M. Ehara, *ChemCatChem* **2017**, 9, 1222; b) H. Xu, C.-Q. Xu, D. Cheng, J. Li, *Cataly. Sci. Technol.* **2017**, 7, 5860; c) J.-X. Liang, X.-F. Yang, A. Wang, T. Zhang, J. Li, *Cataly. Sci. Technol.* **2016**, 6, 6886.

[67] Y. Tang, S. Zhao, B. Long, J.-C. Liu, J. Li, *J. Phys. Chem. C* **2016**, 120, 17514.

[68] X. Zhang, Z. Xia, H. Li, S. Yu, S. Wang, G. Sun, *RSC Adv.* **2019**, 9, 7086.

[69] H. Xu, D. Cheng, D. Cao, X. C. Zeng, *Nat. Catal.* **2018**, 1, 339.

[70] a) H. Thirumalai, J. R. Kitchin, *Top. Cataly.***2018**, 61, 462; b) G. Giannakakis, M. Flytzani-Stephanopoulos, E. C. H. Sykes, *Acc. Chem. Res.***2018**, 52, 237; c) F. R. Lucci, M. T. Darby, M. F. Mattera, C. J. Ivimey, A. J. Therrien, A. Michaelides, M. Stamatakis, E. C. H. Sykes,J. Phys. Chem. Lett. **2016**, 7, 480; d) M. Ruff, N. Takehiro, P. Liu, J. K. Nørskov, R. J. Behm, *ChemPhysChem* **2007**, 8, 2068.

[71] M. T. Darby, R. Réocreux, E. C. H. Sykes, A. Michaelides, M. Stamatakis, *ACS Catal.* **2018**, 8, 5038.

[72] Q. Yue, S. Chang, S. Qin, J. Li, *Phys. Lett. A* **2013**, 377, 1362.

[73] X. Guo, G. Fang, G. Li, H. Ma, H. Fan, L. Yu, C. Ma, X. Wu, D. Deng, M. Wei, *Science* **2014**, 344, 616.

[74] J. H. Kwak, L. Kovarik, J. n. Szanyi, *ACS Catal.* **2013**, 3, 2094.

[75] a) C. Wang, M. Yang, M. Flytzani-Stephanopoulos, *AIChE J.* **2016**, 62, 429; b) H. Guan, J. Lin, B. Qiao, S. Miao, A. Q. Wang, X. Wang, T. Zhang, *AIChE J.* **2017**, 63, 2081.

[76] C. H. Choi, M. Kim, H. C. Kwon, S. J. Cho, S. Yun, H.-T. Kim, K. J. Mayrhofer, H. Kim, M. Choi, *Nat. Commun.* **2016**, 7, 10922.

[77] L.-W. Guo, P.-P. Du, X.-P. Fu, C. Ma, J. Zeng, R. Si, Y.-Y. Huang, C.-J. Jia, Y.-W. Zhang, C.-H. Yan, *Nat. Commun.* **2016**, 7, 13481.

[78] M. M. Schubert, S. Hackenberg, A. C. Van Veen, M. Muhler, V. Plzak, R. J. Behm, *J. Cataly.* **2001**, 197, 113.

[79] a) T. K. Ghosh, N. N. Nair, *ChemCatChem* **2013**, 5, 1811; b) S. F. Hackett, R. M. Brydson, M. H. Gass, I. Harvey, A. D. Newman, K. Wilson, A. F. Lee, *Angew. Chem. Int. Ed.Angew. Chem. Int. Ed.* **2007**, 46, 8593.

[80] I. A. Pašti, B. Johansson, N. V. Skorodumova, Phys. Chem. Chem. Phys. **2018**, 20, 6337.

[81] A. J. Therrien, A. J. Hensley, M. D. Marcinkowski, R. Zhang, F. R. Lucci, B. Coughlin, A. C. Schilling, J.-S. McEwen, E. C. H. Sykes, *Nat. Cataly.* **2018**, 1, 192.

[82] L. Li, A. Wang, B. Qiao, J. Lin, Y. Huang, X. Wang, T. Zhang, *J. Cataly.* **2013**, 299, 90.

[83] X. Sun, J. Lin, Y. Zhou, L. Li, Y. Su, X. Wang, T. Zhang, *AIChE J.* **2017**, 63, 4022.

[84] T. Umebayashi, T. Yamaki, H. Itoh, K. Asai, *J. Phys. Chem. Solids* **2002**, 63, 1909.

[85] T. Wei, Y. Zhu, Y. Wu, X. An, L.-M. Liu, *Langmuir* **2018**, 35, 391.

[86] R. Si, M. Flytzani-Stephanopoulos, *Angew. Chem. Int. Ed.* **2008**, 120, 2926.

[87] L. Nie, D. Mei, H. Xiong, B. Peng, Z. Ren, X. I. P. Hernandez, A. DeLaRiva, M. Wang, M. H. Engelhard, L. Kovarik, *Science* **2017**, 358, 1419.

[88] M. B. Boucher, S. Goergen, N. Yi, M. Flytzani-Stephanopoulos, Phys. Chem. Chem. Phys. **2011**, 13, 2517.

[89] M. B. Boucher, N. Yi, F. Gittleson, B. Zugic, H. Saltsburg, M. Flytzani-Stephanopoulos, *J. Phys. Chem. C* **2010**, 115, 1261.

[90] a) N. Yi, R. Si, H. Saltsburg, M. Flytzani-Stephanopoulos, *Appl. Cataly. B: Environ.* **2010**, 95, 87; b) N. Yi, R. Si, H. Saltsburg, M. Flytzani-Stephanopoulos,Energy Environ. Sci. **2010**, 3, 831.

[91] M. S. Dresselhaus, G. Dresselhaus, P. C. Eklund, *Science of fullerenes and carbon nanotubes: their properties and applications*, Elsevier, **1996**.

[92] a) Y. Zhang, Y. Zhang, D. Zhang, C. Liu, *J. Phys. Chem. B* **2006**, 110, 4671; b) N. W. Shi Kam, T. C. Jessop, P. A. Wender, H. Dai, *J. Ame. Chem. Soc.* **2004**, 126, 6850; c) B. C. Steele, A. Heinzel, in *Materials For Sustainable Energy: A Collection of Peer-Reviewed Research and Review Articles from Nature Publishing Group*, World Sci. **2011**, p. 224; d) M. Lefèvre, J.-P. Dodelet, *Electrochim. Acta* **2003**, 48, 2749.

[93] S. R. Stoyanov, A. V. Titov, P. Král, *Coordination Chemistry Reviews* **2009**, 253, 2852.

[94] a) J. Kim, H. E. Kim, H. Lee, *ChemSusChem* **2018**, 11, 104; b) C. Zhu, S. Fu, Q. Shi, D. Du, Y. Lin, *Angew. Chem. Int. Ed.Angew. Chem. Int. Ed.* **2017**; c) B. Bayatsarmadi, Y. Zheng, A. Vasileff, S. Z. Qiao, *Small* **2017**.

[95] T. Kou, T. Smart, B. Yao, I. Chen, D. Thota, Y. Ping, Y. Li, *Adv. Energy Mater.* **2018**, 8, 1703538.

[96] a) X. Cui, J. Xiao, Y. Wu, P. Du, R. Si, H. Yang, H. Tian, J. Li, W. H. Zhang, D. Deng, *Angew. Chem. Int. Ed.Angew. Chem. Int. Ed.* **2016**, 55, 6708; b) A. Zitolo, N. Ranjbar-Sahraie, T. Mineva, J. Li, Q. Jia, S. Stamatin, G. F. Harrington, S. M. Lyth, P. Krtil, S. Mukerjee, *Nat. Commun.***2017**, 8, 957; c) M. Li, S. Wu, X. Yang, J. Hu, L. Peng, L. Bai, Q. Huo, J. Guan, *Appl. Catal. A Gen.***2017**, 543, 61; d) L. Yang, L. Shi, D. Wang, Y. Lv, D. Cao, *Nano Energy* **2018**, 50, 691.

[97] a) Y. Chen, S. Ji, Y. Wang, J. Dong, W. Chen, Z. Li, R. Shen, L. Zheng, Z. Zhuang, D. Wang, *Angew. Chem. Int. Ed.* **2017**, 129, 7041; b) A. Zitolo, V. Goellner, V. Armel, M.-T. Sougrati, T. Mineva, L. Stievano, E. Fonda, F. Jaouen, *Nat. Mater.* **2015**, 14, 937.

[98] G. Gao, Y. Jiao, E. R. Waclawik, A. Du, *J. Ame. Chem. Soc.* **2016**, 138, 6292.

[99] H. Wu, H. Li, X. Zhao, Q. Liu, J. Wang, J. Xiao, S. Xie, R. Si, F. Yang, S. Miao,Energy Environ. Sci. **2016**, 9, 3736.

[100] N. Cheng, S. Stambula, D. Wang, M. N. Banis, J. Liu, A. Riese, B. Xiao, R. Li, T.-K. Sham, L.-M. Liu, *Nat. Commun.* **2016**, 7, 13638.

[101] W. H. Lai, B. W. Zhang, Z. Hu, X. M. Qu, Y. X. Jiang, Y. X. Wang, J. Z. Wang, H. K. Liu, S. L. Chou, *Adv. Funct. Mater.* **2019**, 1807340.
[102] J. A. Rodriguez, D. W. Goodman, *Science* **1992**, 257, 897.
[103] F. A. Cotton, C. A. Murillo, R. A. Walton, *Multiple bonds between metal atoms*, Springer Science & Business Media, **2005**.
[104] M. T. Greiner, T. Jones, S. Beeg, L. Zwiener, M. Scherzer, F. Girgsdies, S. Piccinin, M. Armbrüster, A. Knop-Gericke, R. Schlögl, *Nat. Chem.* **2018**, 10, 1008.
[105] M. D. Marcinkowski, M. T. Darby, J. Liu, J. M. Wimble, F. R. Lucci, S. Lee, A. Michaelides, M. Flytzani-Stephanopoulos, M. Stamatakis, E. C. H. Sykes, *Nat. Chem.* **2018**, 10, 325.
[106] J. Liu, F. R. Lucci, M. Yang, S. Lee, M. D. Marcinkowski, A. J. Therrien, C. T. Williams, E. C. H. Sykes, M. Flytzani-Stephanopoulos, *J. Ame. Chem. Soc.* **2016**, 138, 6396.
[107] Y. T. Kim, K. Ohshima, K. Higashimine, T. Uruga, M. Takata, H. Suematsu, T. Mitani, *Angew. Chem. Int. Ed.* **2006**, 118, 421.
[108] M. Yang, S. Li, Y. Wang, J. A. Herron, Y. Xu, L. F. Allard, S. Lee, J. Huang, M. Mavrikakis, M. Flytzani-Stephanopoulos, *Science* **2014**, 346, 1498.
[109] M. Yang, J. Liu, S. Lee, B. Zugic, J. Huang, L. F. Allard, M. Flytzani-Stephanopoulos, *J. Ame. Chem. Soc.* **2015**, 137, 3470.
[110] a) R. Bliem, J. E. van der Hoeven, J. Hulva, J. Pavelec, O. Gamba, P. E. de Jongh, M. Schmid, P. Blaha, U. Diebold, G. S. Parkinson, *P NaAS* **2016**, 113, 8921; b) S. Horch, H. Lorensen, S. Helveg, E. Lægsgaard, I. Stensgaard, K. W. Jacobsen, J. K. Nørskov, F. Besenbacher, *Nature* **1999**, 398, 134.
[111] a) L. Zhang, A. Wang, W. Wang, Y. Huang, X. Liu, S. Miao, J. Liu, T. Zhang, *ACS Catal.* **2015**, 5, 6563; b) W. Liu, L. Zhang, W. Yan, X. Liu, X. Yang, S. Miao, W. Wang, A. Wang, T. Zhang, *Chem. Sci.* **2016**, 7, 5758.
[112] P. Hu, Z. Huang, Z. Amghouz, M. Makkee, F. Xu, F. Kapteijn, A. Dikhtiarenko, Y. Chen, X. Gu, X. Tang, *Angew. Chem. Int. Ed.***2014**, 126, 3486.
[113] H. Wei, Y. Ren, A. Wang, X. Liu, X. Liu, L. Zhang, S. Miao, L. Li, J. Liu, J. Wang, *Chem. Sci.* **2017**, 8, 5126.
[114] a) G. X. Pei, X. Y. Liu, A. Wang, A. F. Lee, M. A. Isaacs, L. Li, X. Pan, X. Yang, X. Wang, Z. Tai, *ACS Catal.* **2015**, 5, 3717; b) Q. Feng, S. Zhao, Y. Wang, J. Dong, W. Chen, D. He, D. Wang, J. Yang, Y. Zhu, H. Zhu, *J. Ame. Chem. Soc.* **2017**, 139, 7294.
[115] J. H. Kwak, L. Kovarik, J. n. Szanyi, *ACS Catal.***2013**, 3, 2449.
[116] J. C. Matsubu, V. N. Yang, P. Christopher, *J. Ame. Chem. Soc.* **2015**, 137, 3076.
[117] a) M.-J. Cheng, E. L. Clark, H. H. Pham, A. T. Bell, M. Head-Gordon, *ACS Catal.***2016**, 6, 7769; b) S. Back, J. Lim, N.-Y. Kim, Y.-H. Kim, Y. Jung, *Chem. Sci.* **2017**, 8, 1090; c) S. Sarfraz, A. T. Garcia-Esparza, A. Jedidi, L. Cavallo, K. Takanabe, *ACS Catal.* **2016**, 6, 2842; d) H. B. Yang, S.-F. Hung, S. Liu, K. Yuan, S. Miao, L. Zhang, X. Huang, H.-Y. Wang, W. Cai, R. Chen, *Nat. Energy* **2018**, 3, 140.
[118] C. Genovese, M. E. Schuster, E. K. Gibson, D. Gianolio, V. Posligua, R. Grau-Crespo, G. Cibin, P. P. Wells, D. Garai, V. Solokha, *Nat. Commun.***2018**, 9, 935.
[119] S. Siahrostami, A. Verdaguer-Casadevall, M. Karamad, D. Deiana, P. Malacrida, B. Wickman, M. Escudero-Escribano, E. A. Paoli, R. Frydendal, T. W. Hansen, *Nat. Mater.* **2013**, 12, 1137.
[120] A. Verdaguer-Casadevall, D. Deiana, M. Karamad, S. Siahrostami, P. Malacrida, T. W. Hansen, J. Rossmeisl, I. Chorkendorff, I. E. Stephens, *Nano Lett.* **2014**, 14, 1603.
[121] H. Yan, H. Lv, H. Yi, W. Liu, Y. Xia, X. Huang, W. Huang, S. Wei, X. Wu, J. Lu, *J. Cataly.* **2018**, 366, 70.

[122] Z. Li, T. He, D. Matsumura, S. Miao, A. Wu, L. Liu, G. Wu, P. Chen, *ACS Catal.* **2017**, 7, 6762.
[123] J. Shan, J. Liu, M. Li, S. Lustig, S. Lee, M. Flytzani-Stephanopoulos, *Appl. Cataly. B: Environ.* **2018**, 226, 534.
[124] C. H. Chen, D. Wu, Z. Li, R. Zhang, C. G. Kuai, X. R. Zhao, C. K. Dong, S. Z. Qiao, H. Liu, X. W. Du, *Adv. Energy Mater.* **2019**, 1803913.
[125] a) R. Long, Y. Li, Y. Liu, S. Chen, X. Zheng, C. Gao, C. He, N. Chen, Z. Qi, L. Song, *J. Ame. Chem. Soc.* **2017**, 139, 4486; b) X. L. Du, X. L. Wang, Y. H. Li, Y. L. Wang, J. J. Zhao, L. J. Fang, L. R. Zheng, H. Tong, H. G. Yang, *Chem. Commun.* **2017**, 53, 9402.
[126] M. D. Marcinkowski, A. D. Jewell, M. Stamatakis, M. B. Boucher, E. A. Lewis, C. J. Murphy, G. Kyriakou, E. C. H. Sykes, *Nat. Mater.* **2013**, 12, 523.
[127] R. Shi, C. Tian, X. Zhu, C.-Y. Peng, B. Mei, L. He, X.-L. Du, Z. Jiang, Y. Chen, S. Dai, *Chem. Sci.* **2019**, 10, 2585.
[128] J.-X. Liang, J. Lin, X.-F. Yang, A.-Q. Wang, B.-T. Qiao, J. Liu, T. Zhang, J. Li, *J. Phys. Chem. C* **2014**, 118, 21945.
[129] X. Li, X. Huang, S. Xi, S. Miao, J. Ding, W. Cai, S. Liu, X. Yang, H. Yang, J. Gao, *J. Ame. Chem. Soc.* **2018**, 140, 12469.
[130] L. Jiao, G. Wan, R. Zhang, H. Zhou, S. H. Yu, H. L. Jiang, *Angew. Chem. Int. Ed.* **2018**, 57, 8525.

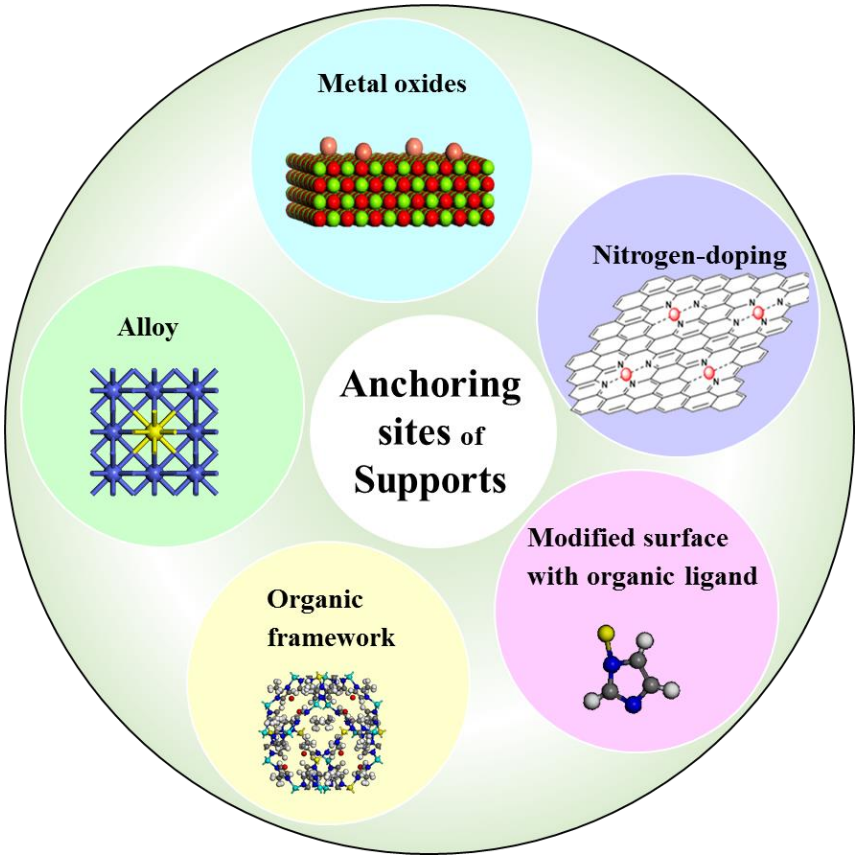

Figure 1. Schematic diagrams illustrate different types of surface of supports: metal oxide, nitrogen doped carbon, modified surface with organic ligand, organic framework, and alloy.

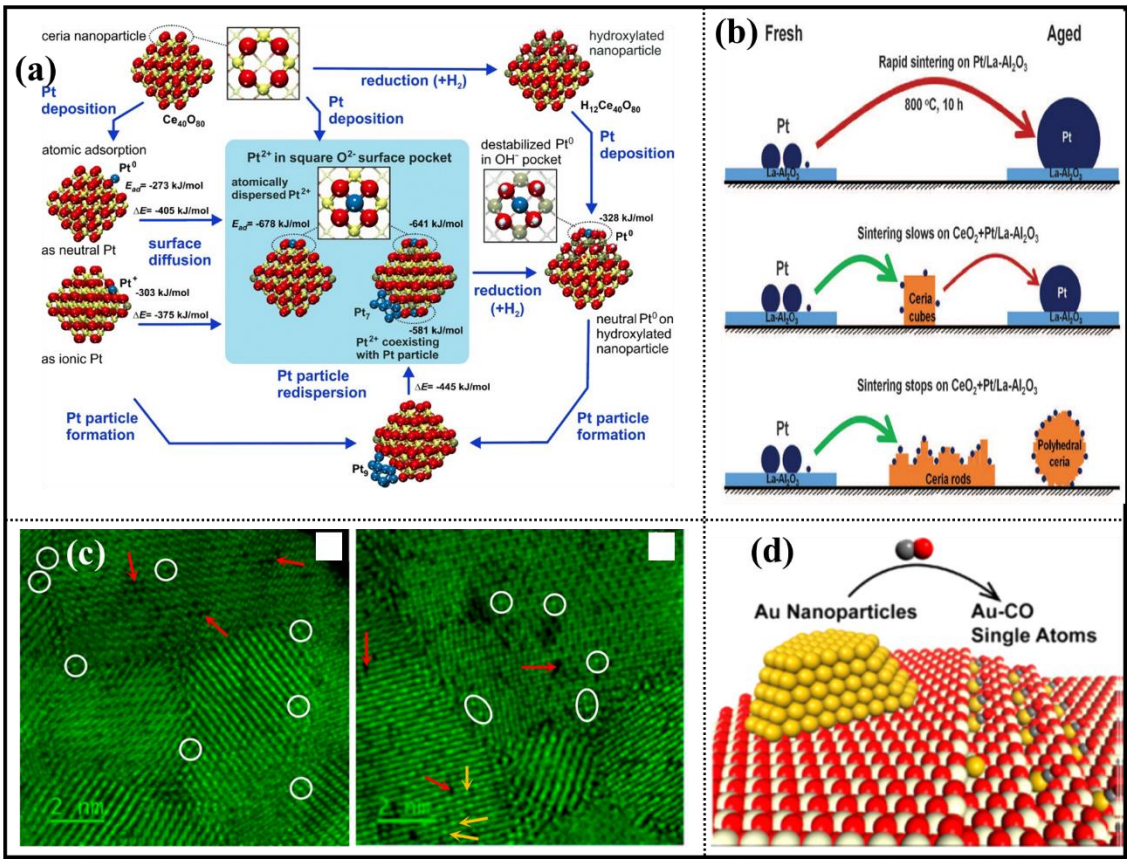

Figure 2. (a) Structure and energetics of the anchored Pt^{2+} species on ceria nanoparticles determined by theory. Reproduced with permission.[37] Copyright 2014, Wiley-VCH. (b) Illustration of Pt nanoparticle sintering, showing how ceria can trap the mobile Pt to suppress sintering. Cubes appear to be less effective than rods or polyhedral ceria. Reproduced with permission.[7c] Copyright 2016, American Association for the Advancement of Science (AAAS). (c) HAADF-STEM images of $0.05Au_1/CeO_2$. Reproduced with permission.[7a] Copyright 2015, American Chemical Society. (d) Illustration of the different ability on oxidizing CO via altering the relative chemical potentials between SAs and metal nanoparticles (NPs) on ceria. Reproduced with permission.[40] Copyright 2017, American Chemical Society.

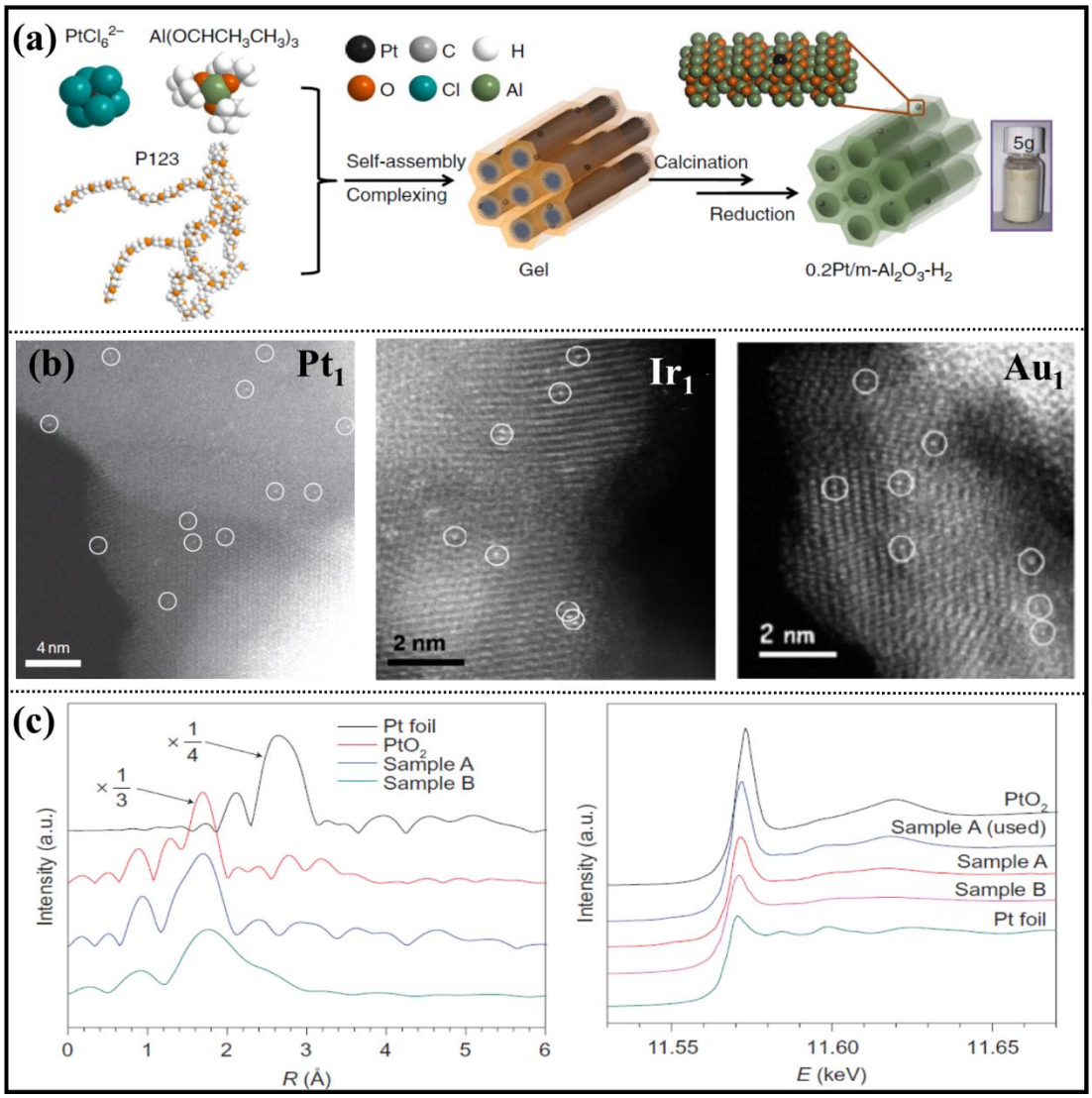

Figure 3. (a) Schematic illustration of the 0.2Pt/m-Al_2O_3-H_2 synthesis process via a sol-gel solvent vaporization self-assembly method. Reproduced with permission.[8b] Copyright 2017, Nature Publishing Group. (b) HAADF-STEM images of Pt_1/FeO_x sample, Ir_1/FeO_x, and Au_1/FeO_x sample. Reproduced with permission.[2] Copyright 2011, Nature Publishing Group; Reproduced with permission.[42] Copyright 2014, American Chemical Society; Reproduced with permission.[9b] Copyright 2015, Springer. (c) The k3-weighted Fourier transform spectra (the above) and the normalized XANES spectra (the bottom) of sample A (Pt_1/FeO_x), sample B (Pt_1/FeO_x with loading mass of 2.5 wt. % Pt), PtO_2 and Pt foil. Reproduced with permission.[2] Copyright 2011, Nature Publishing Group.

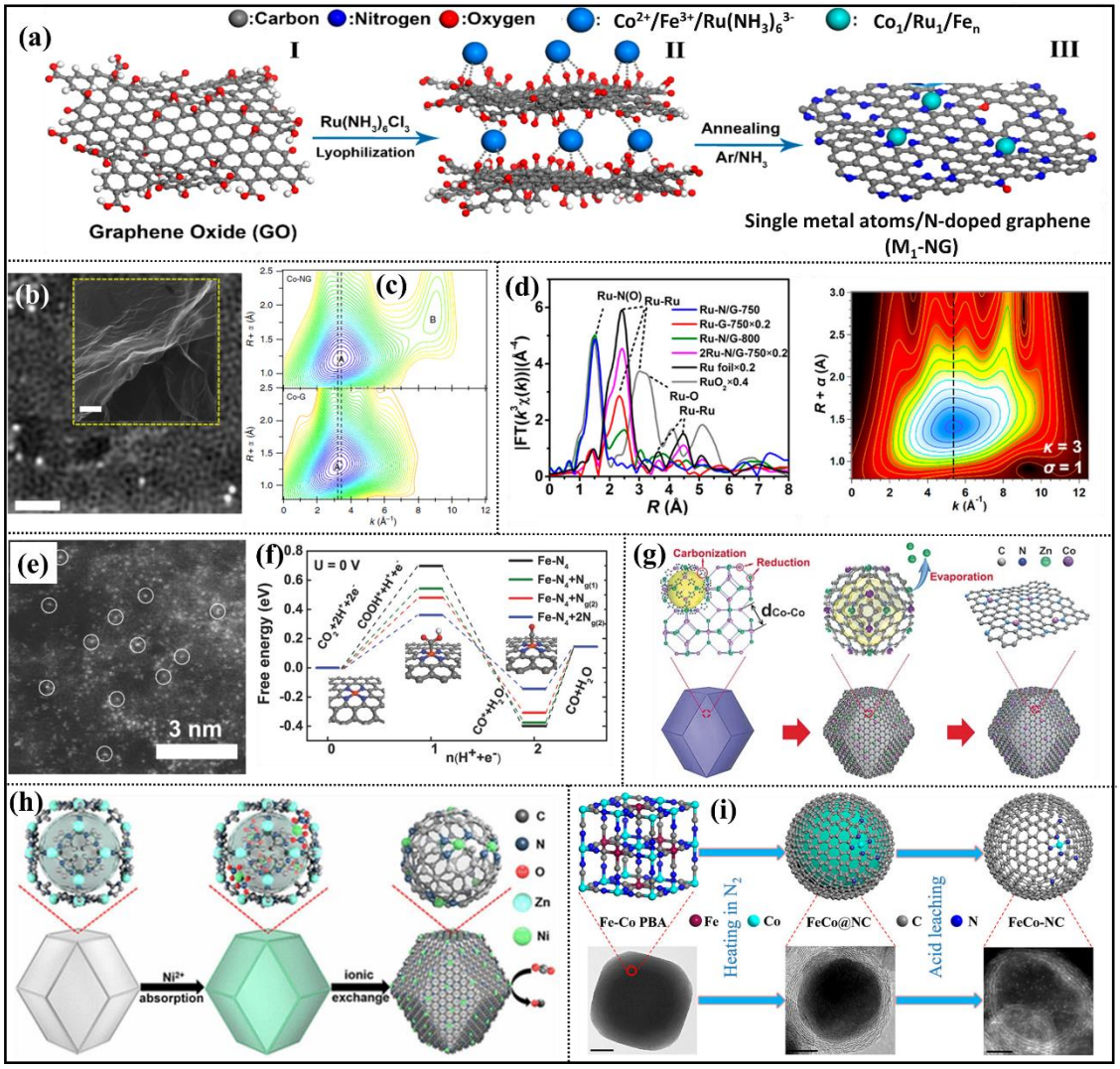

Figure 4. (a) Schematic illustration of the synthetic process for the $Ru_1/Co_1/Fe_n$ catalysts on nitrogen-doped graphene (NG). Reproduced with permission.[21a] Copyright 2015, Nature Publishing Group; Reproduced with permission.[21b] Copyright 2017, American Chemical Society; Reproduced with permission.[48] Copyright 2018, Wiley-VCH; respectively. (b) STEM image of Co_1-NG, inset is the SEM image of NG. (c) Left: Wavelet transforms for the Co_1-NG and Co-containing graphene (Co-G). Reproduced with permission.[21a] Copyright 2015, Nature Publishing Group. Right: Fourier transform magnitudes of the experimental Ru K-edge EXAFS spectra of the Ru-N/G samples prepared under different conditions along with reference materials. (d) The Fourier transforms are not corrected for phase shift. WT for the

k^3-weighted EXAFS signal of sample Ru-N/G-750. The maximum at 5.5 $Å^{-1}$ is associated with the Ru-N(O) contributions. Reproduced with permission.[21b] Copyright 2017, American Chemical Society and (e) The STEM image of high density atomic Fe dispersion on NG. Reproduced with permission.[48] Copyright 2018, Wiley-VCH (f) Theoretical calculations and proposed mechanism on the nitrogen-coordinated Fe catalytic site.[48] Copyright 2018, Wiley-VCH. (g) The schematic illustration of the formation of Co_1/*N*-C (900). Reproduced with permission.[23a] Copyright 2016, Wiley-VCH. (h) Schematic illustration of the synthetic process for the Fe-SAs/CN and Ni-SAs/CN. Reproduced with the permission.[24a] Copyright 2017, American Chemical Society; (i) Schematic illustration of the synthetic process for single-Co-atom catalysts via pyrolyzing Fe-Co prussian blue analogue. Reproduced with the permission.[129] Copyright 2018, American Chemical Society.

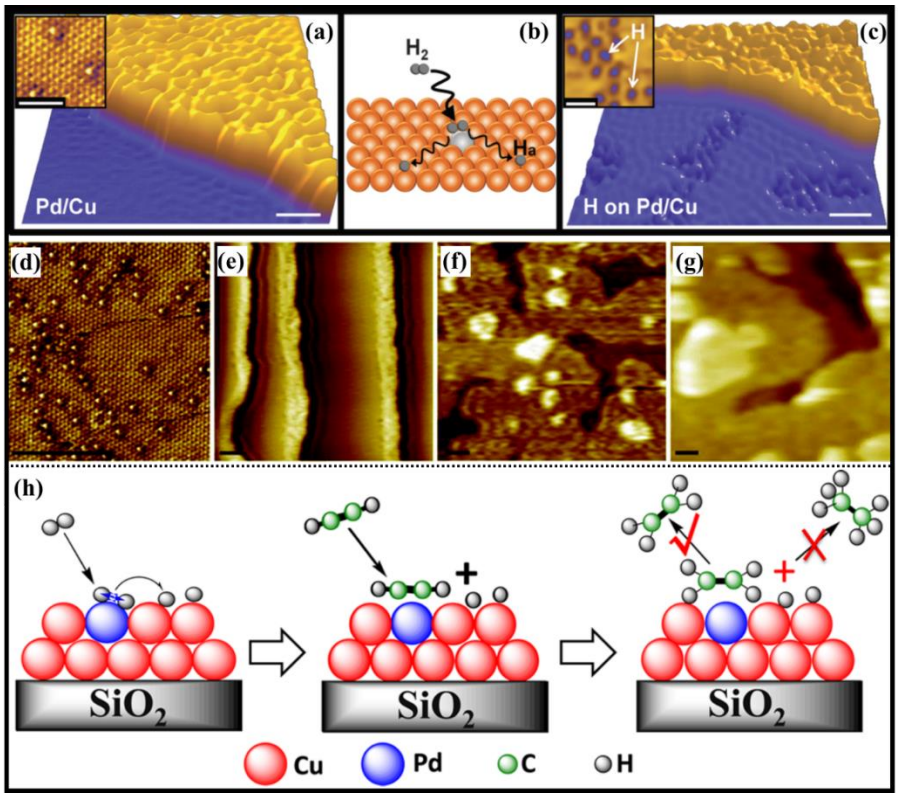

Figure 5. STM images showing atomically dispersed Pd atoms in a Cu(111) surface and hydrogen atoms that have dissociated and spilled over onto the Cu surface. (a) Pd alloys into the Cu(111) surface preferentially above the step edges as evidenced by the rumpled appearance of the upper terrace (scale bar indicates 5 nm). (Inset) Atomic resolution of the Pd/Cu alloy on the upper terrace showing individual, isolated Pd atoms in the surface layer appearing as protrusions (scale bar, 2 nm). (b) Schematic showing H_2 dissociation and spillover at individual, isolated Pd atom sites in the Cu surface layer. (c) Islands of H atoms imaged after hydrogen uptake appear as depressed regions on the clean Cu(111) lower terrace (scale bar, 5 nm). (Inset) High-resolution image of individual hydrogen atoms on Cu(111) (scale bar, 2 nm). Reproduced with permission. [27a] Copyright 2012, American Association for the Advancement of Science (AAAS). (d-g) STM images of Pd/Cu alloys with a range of stoichiometries: (d) 0.01 ml Pd, (e) 0.1 ml Pd, (f) 1 ml Pd and (g) 2 ml Pd. Scale bars: 5nm. Pd/Cu alloys were formed at 380 K. Reproduced with permission.[27b] Copyright 2013, Royal Society of

Chemistry. (h) Proposed reaction pathway for semi-hydrogenation of acetylene over silica-supported Cu alloyed Pd SAC. Reproduced with permission.[27d] Copyright 2017, American Chemical Society.

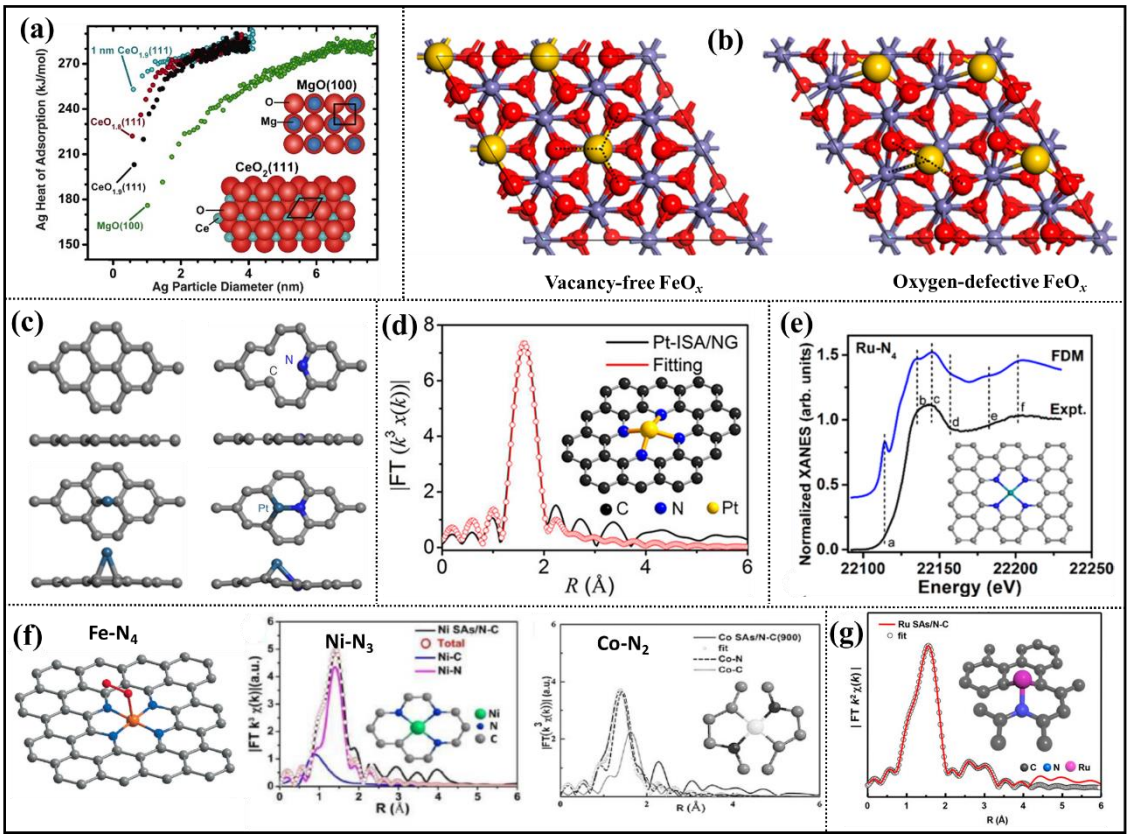

Figure 6. (a) Measured heat of Ag atom adsorption for these four surfaces plotted versus the average Ag particle diameter. The inset shows structural models for perfect CeO_2(111) and MgO(100), with their unit cells in black lines. Reproduced with permission.[59] Copyright 2010, American Association for the Advancement of Science (AAAS). (b) Top views of M_1 (M = Au, Rh, Pd, Co, Cu, and Ru) anchored on vacancy-free and oxygen-defective iron-oxide surfaces. Reproduced with permission.[61] Copyright 2014, American Chemical Society. (c) Optimized structures of different substrates: Pristine graphene (g) Pyridinic N_1-doped graphene (g-P-N_1). Optimized structures of Pt adsorption on pristine graphene (g-Pt), and Pt adsorption on g-P-N_1 (g-P-N_1-Pt). The grey, blue and cyan balls denote the carbon, nitrogen and platinum atoms, respectively. Reproduced with permission.[21a] Copyright 2015, Nature Publishing Group. (d)

The EXAFS fitting curves of Pt-ISA/NG at R space. Reproduced with permission.[62] Copyright 2018, American Chemical Society. (e) Comparison between the experimental Ru K-edge XANES spectrum of Ru-N/G-750 and the theoretical spectrum calculated from the depicted structures using the full-potential FDM. Reproduced with permission.[21b] Copyright 2017, American Chemical Society. (f) The proposed Co/Ni/Fe-N_x−C architectures. Reproduced with permission.[23a] Copyright 2016, Wiley-VCH; Reproduced with permission.[24a] Copyright 2017, American Chemical Society; Reproduced with permission.[24b] Copyright 2017, Wiley-VCH. (g) The fitting results of the EXAFS spectra of Ru SAs/N−C. Reproduced with permission.[25] Copyright 2017, American Chemical Society.

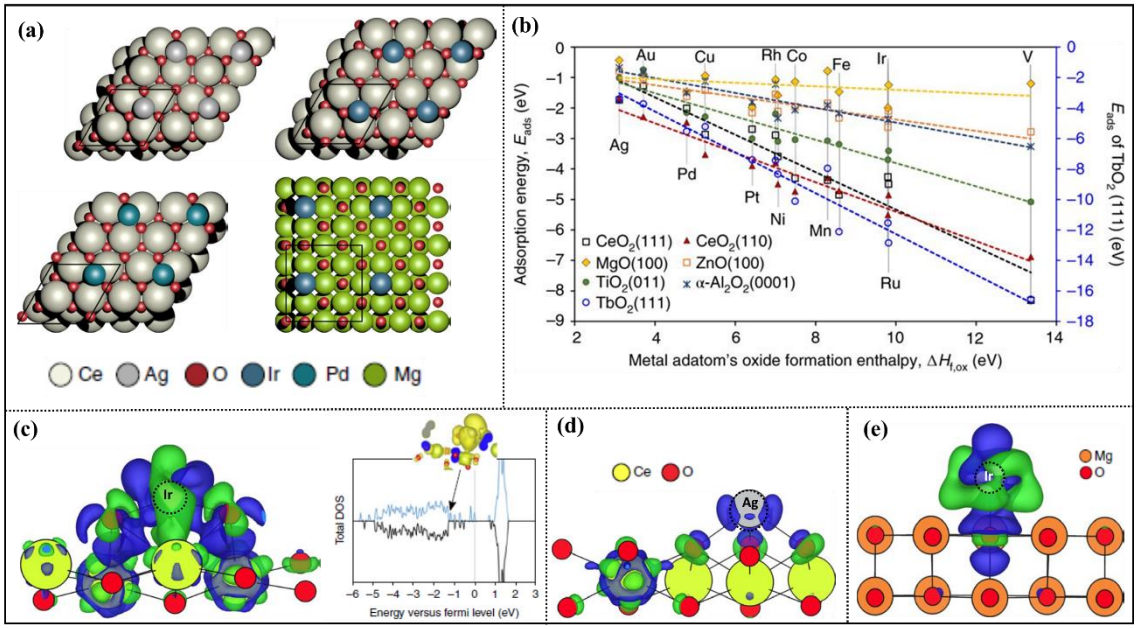

Figure 7. (a) Top view of adsorption geometries of single metals for Ag at the threefold hollow site (left top), Ir at twofold oxygen bridge site (right top), Pd at oxygen side-bridge site on CeO_2(111) (left bottom), and adsorbed metals at preferable anionic oxygen site on MgO(100) (right bottom). (b) Correlation between metal/support adsorption energies and metal adatom's oxide formation enthalpy. (c) Isostructural charge density difference plots via metal-support interactions of Ir/CeO_2(111), (d) Ag/CeO_2(111), and (e) Ir/MgO(100). Reproduced with the permission.[65] Copyright 2018, Nature Publishing Group.

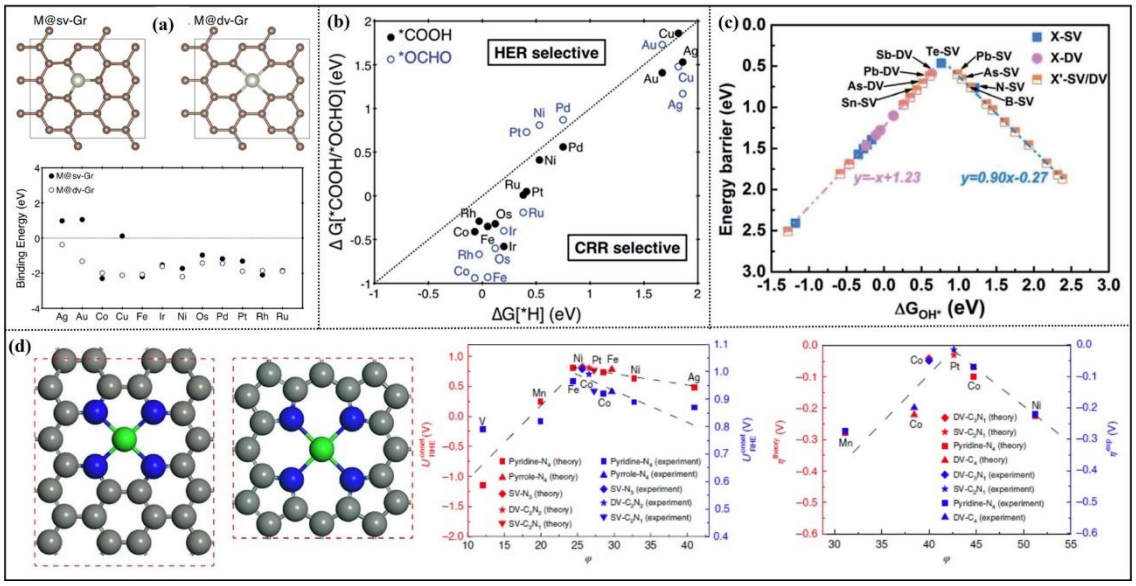

Figure 8. (a) The top view of single atom on single vacancy-graphene (Top left) and single atom on double vacancy-graphene, binding energies of various transition metal atoms with the sv-Gr (filled black circles) and dv-Gr (open blue circles) defective sites (Bottom). (b) Free energy change of the first protonation step in the CO_2 reduction reaction (CRR) and H_2 evolution reaction (HER) on the various SACs. Reproduced with permission.[117b] Copyright 2017, Royal society of chemistry. (c) The "volcanic curve" relationship between ΔG_{OH*} and energy barrier for selected catalysts. Reproduced with permission.[68] Copyright 2019, Royal society of chemistry. (d) Single vacancy with four pyridine nitrogen atoms (pyridine-N4) (Left 1) and four pyrrole nitrogen atoms (pyrrole-N4) (Left 2). The green, blue and grey colours represent TM, N and C atoms, respectively. Theoretical and corresponding experimental onset potentials for ORR versus the descriptor φ (Left 3).Theoretical and corresponding experimental overpotentials for HER versus the descriptor φ (Right). Reproduced with permission.[69] Copyright 2018, Nature Publishing Group.

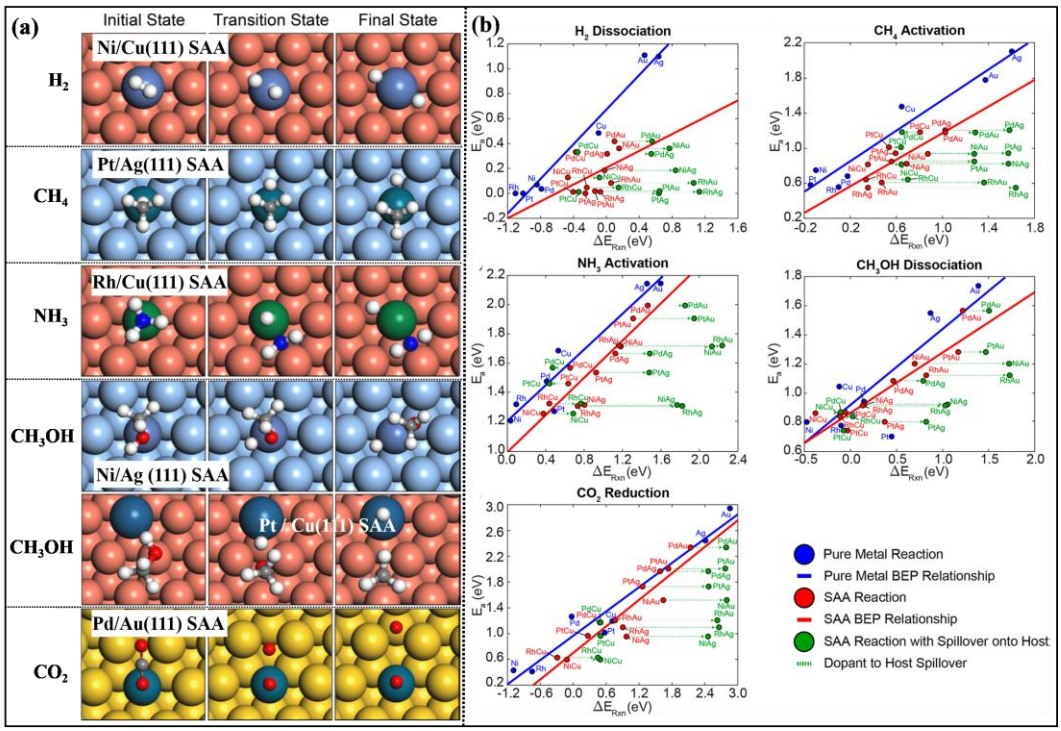

Figure 9. (a) The top view of optimized structure of single atom based alloy: Ni/Cu(111), Pd/Ag(111),Rh/Cu(111), Ni/Ag(111), Pd/Au(111). (b) Brønsted−Evans−Polanyi relationships for five simple catalytic bond scissions on pure metal (111) surfaces (blue) and SAA (111) surfaces (red). Reproduced with permission.[71] Copyright 2018, American Chemical Society.

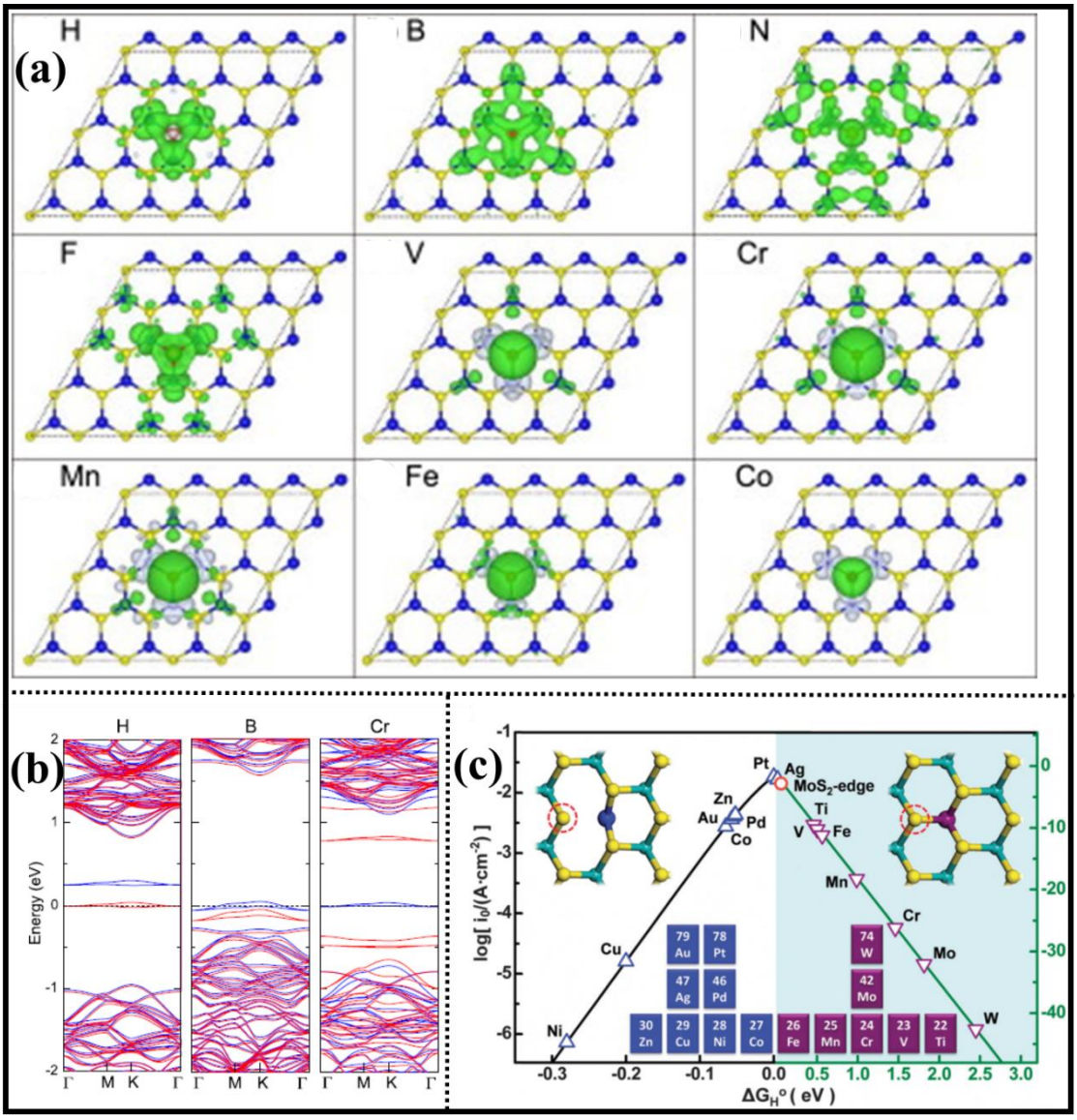

Figure 10. (a) Spin density isosurfaces of substituted 1H-MoS_2 with different atoms.[72] Copyright 2013, Elservier. (b) Band structures of H, B and Cr-substituted MoS_2, with red (blue) color corresponding to up-spin (down-spin) channel. Reproduced with permission.[72] Copyright 2013, Elservier. (c) The relation between currents ($\log(i_0)$) and ΔG_H^0 presents a volcano curve. Reproduced with permission.[49a] [17a]Copyright 2015, Royal Society of Chemistry.

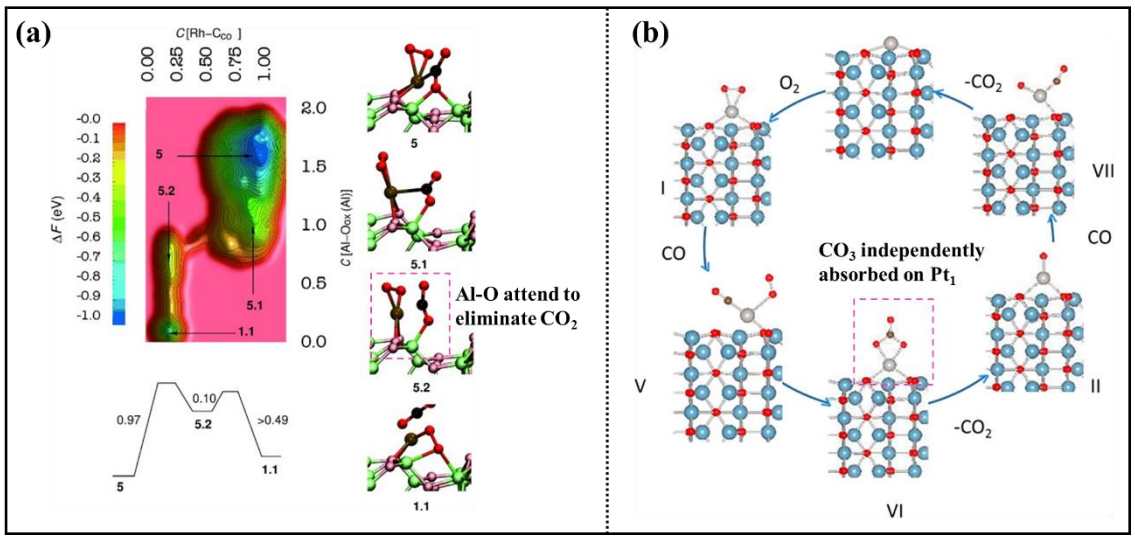

Figure 11. (a) Reconstructed free energy surface, free energy profile, and snapshots from the metadynamics simulation of 5→1.1, The pink box shows that the single atom Ru_1 absorbs O^2 while the Al-O attend to eliminate CO_2. Reproduced with permission.[79a] Copyright 2013, Wiley-VCH; (b) Pathway for CO Oxidation on Single Pt Atoms Supported on the (010) Surface of θ-Al_2O_3. Reproduced with permission. [8a] Copyright 2013, American Chemical Society.

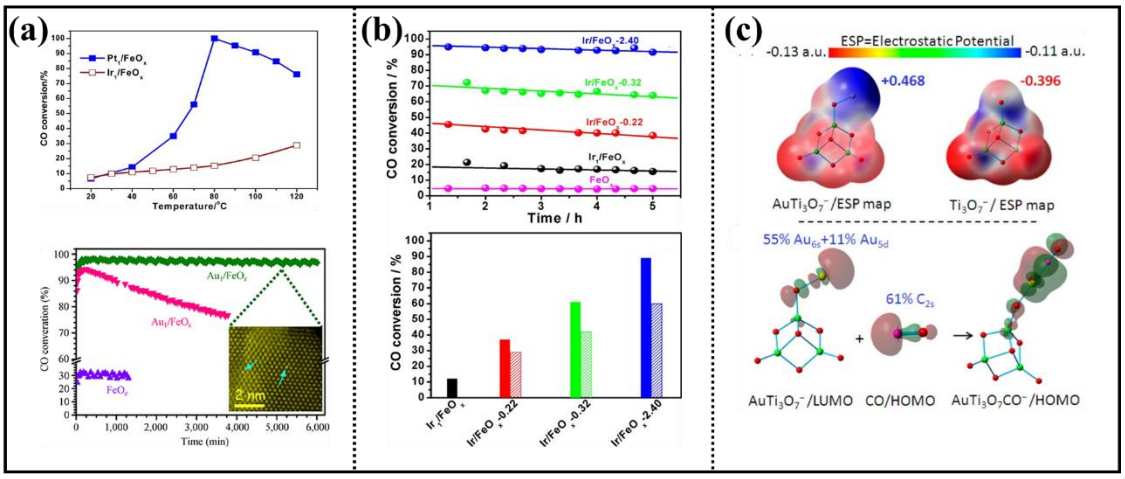

Figure 12. (a) The conversion efficiency of CO of single atom catalysts Pt_1, Ir_1, and Au_1 on FeO_X. Reproduced with permission.[42] Copyright 2014, American Chemical Society; Reproduced with permission.[9b] Copyright 2015, Springer. (b) CO conversions at 300 °C on the Ir/FeO_x catalysts with different Ir loadings. Reproduced with permission.[9a] Copyright 2013, American Chemical Society. (b) Electrostatic potential maps for clusters $AuTi_3O_7^-$ and $Ti_3O_7^-$ and DFT calculated molecular orbitals for $AuTi_3O_7^-$ (LUMO), CO (HOMO), and

$AuTi_3O_7CO^-$ (HOMO). 1 au = 27.2114 V. Reproduced with permission.[43] Copyright 2014, American Chemical Society.

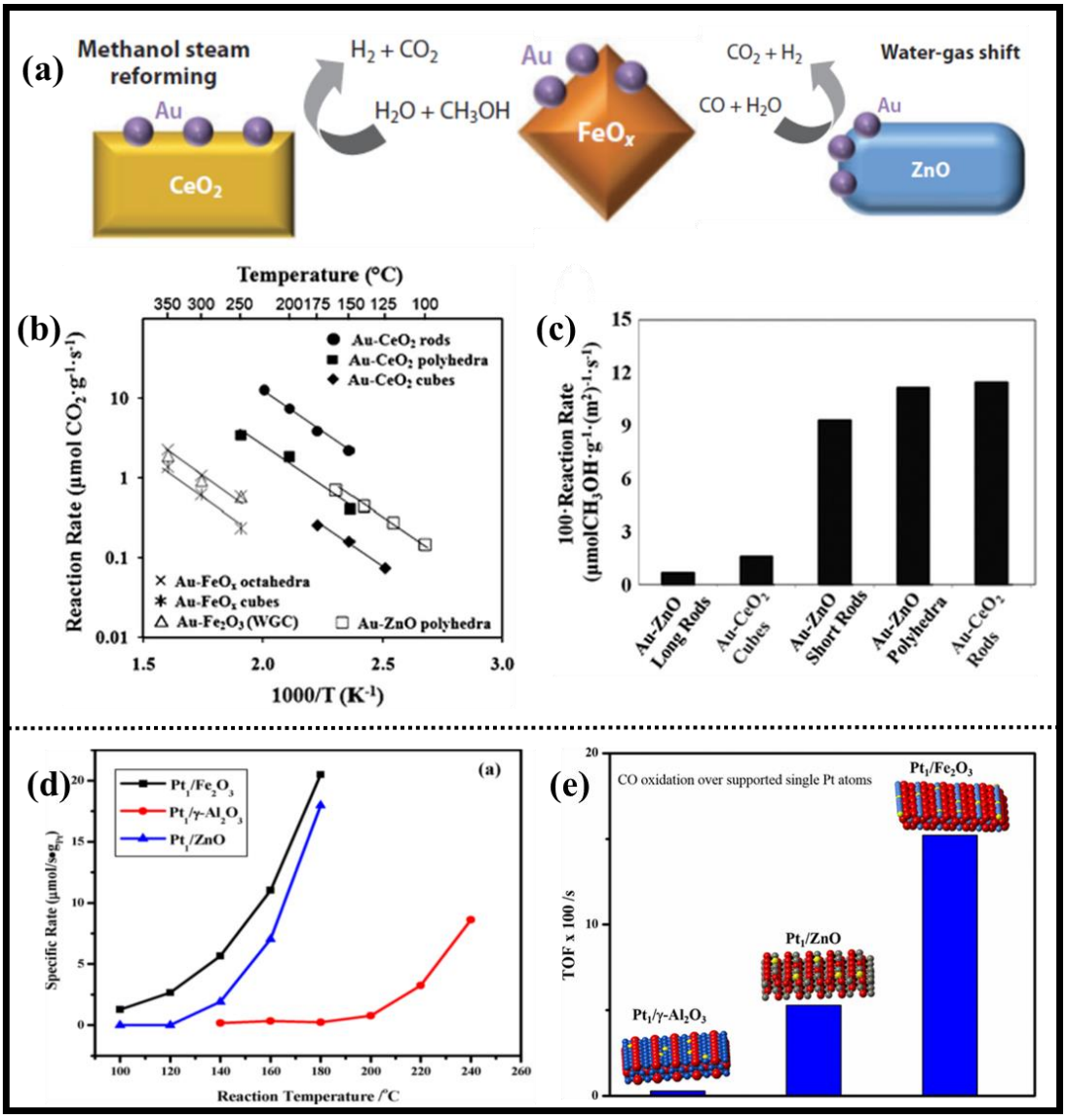

Figure 13. (a) The schematic illustration of Au catalysts on different supports: CeO_2, FeO_x, and ZnO for methanol steam reforming and water-gas shift; (b) Steady-state WGS reaction rates over gold–metal oxide catalysts on various substrates; (c) Comparison of SRM rates at 250 °C over Au–ZnO and Au–CeO_2 nanoshapes. Reproduced with permission.[88] Copyright 2011, Royal Society of Chemistry. (d) Specific rate of wet CO oxidation over dry Pt_1/Fe_2O_3, Pt_1/ZnO, and Pt_1/γ-Al_2O_3 SACs; (e) The turn over frequency (TOF) comparison of Pt_1 single atoms on

different metal oxide supports for dry CO oxidation at 140 °C. Reproduced with permission.[33] Copyright 2017, American Chemical Society.

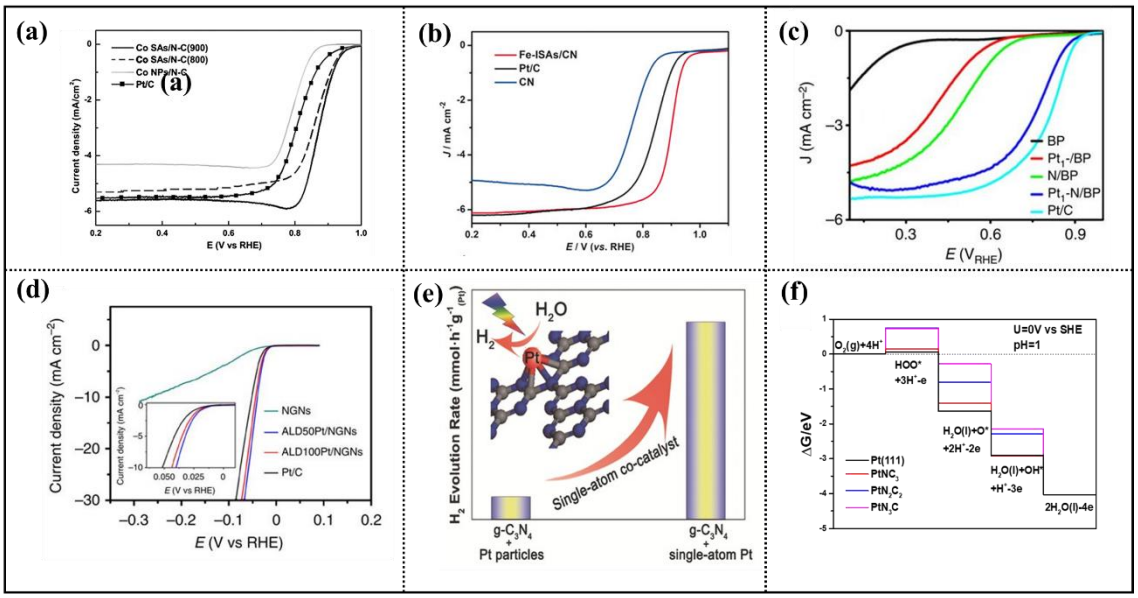

Figure 14. (a-c) The ORR polarization curves of single atom catalysts: Co_1, Fe_1, and Pt_1on nitrogen doped carbon. Reproduced with permission. [23a] Copyright 2016, Wiley-VCH; Reproduced with permission. [130] Copyright 2018, Wiley-VCH; Reproduced with permission. [21c] Copyright 2017, Nature Publishing Group. (d-e) The HER polarization curves of single atoms Pt_1 on nitrogen doped carbon[100] and C_3N_4 framework respectively[22b]. Copyright 2016, Nature Publishing Group; Copyright 2016, Wiley-VCH. (f) Free energy diagram of ORR on $PtNC_3$, PtN_2C_2, PtN_3C, and Pt(111). Reproduced with permission. [101] Copyright 2019, Wiley-VCH.

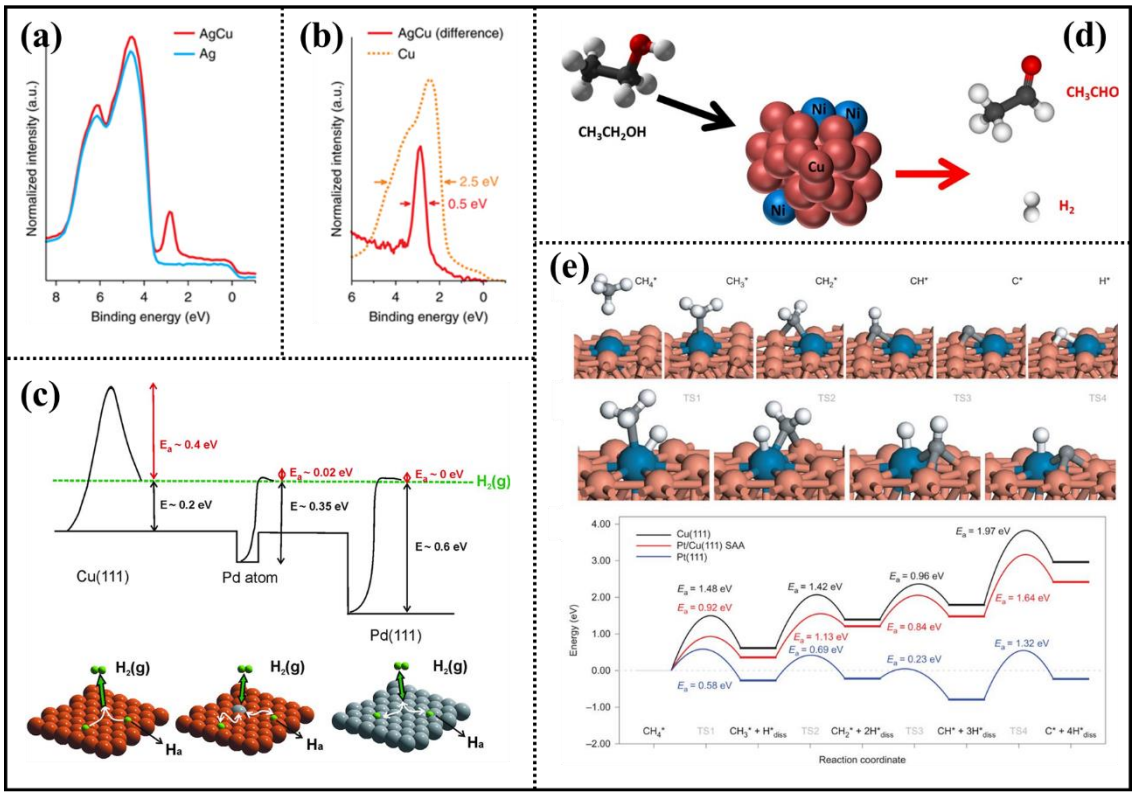

Figure 15. (a) The measured valence photoemission spectra (hν = 150 eV) of an AgCu alloy that contained 0.3 at% Cu and metallic Ag reveal the narrow Cu 3d states at a binding energy of ~2.5 eV. (b) The difference spectrum of AgCu and Ag, plotted with a Cu reference spectrum, demonstrate that the Cu 3d states in AgCu are one-fifth the width they are in bulk Cu. Reproduced with permission.[104] Copyright 2018, Nature Publishing Group. (c) Potential energy diagram depicting the mode of action of a Pd SAA surface compared with those of pure Cu(111) and Pd(111). Reproduced with permission. [27a] Copyright 2012, American Association for the Advancement of Science (AAAS). (d) The illustration of the conversion process of dehydrogenation of ethanol to acetaldehyde and hydrogen on highly dilute NiCu alloys. Reproduced with permission.[27e] Copyright 2017, Elsevier. (e) Optimized configurations from DFT for the most stable adsorptions of C_xH_y species ($x = 0,1$; $y = 0,1,2,3,4$) on the Pt/Cu(111) SAA surface (Top) and the transition states (TSs) (Middle), and energy landscape for the full dehydrogenation of adsorbed CH_4* on Cu(111) (black), Pt/Cu(111) SAA

(red) and Pt(111) (blue) (bottom). Reproduced with permission.[105] Copyright 2017, Nature Publishing Group.

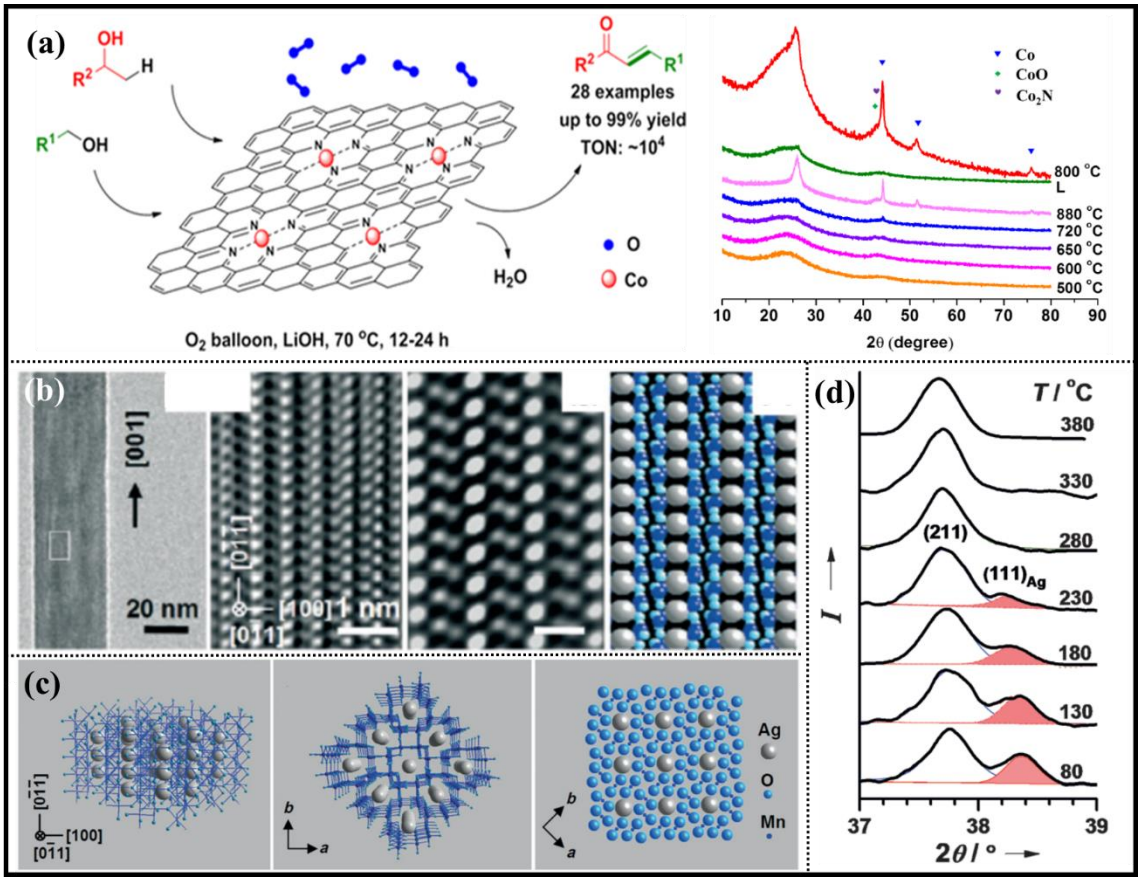

Figure 16. (a) The proposed Co-N-C architecture toward the target reactions and stability of this catalyst paralysed at different temperatures and acid leaching. Reproduced with permission.[111a] Copyright 2015, American Chemical Society. (b) TEM image and HRTEM images of a Ag-HMO nanorod with a [001] growth direction with Auto-correlation function analysis showing a corresponding simulated image; (c) Single-atom Ag chains inside the tunnels of the HMO viewed from the [011] and [001] directions, respectively, and atom arrangement on the (001) facet of Ag-HMO; (d) in situ XRD patterns of the formation of Ag-HMO at different temperature. Reproduced with permission.[13] Copyright 2012, Wiley-VCH.

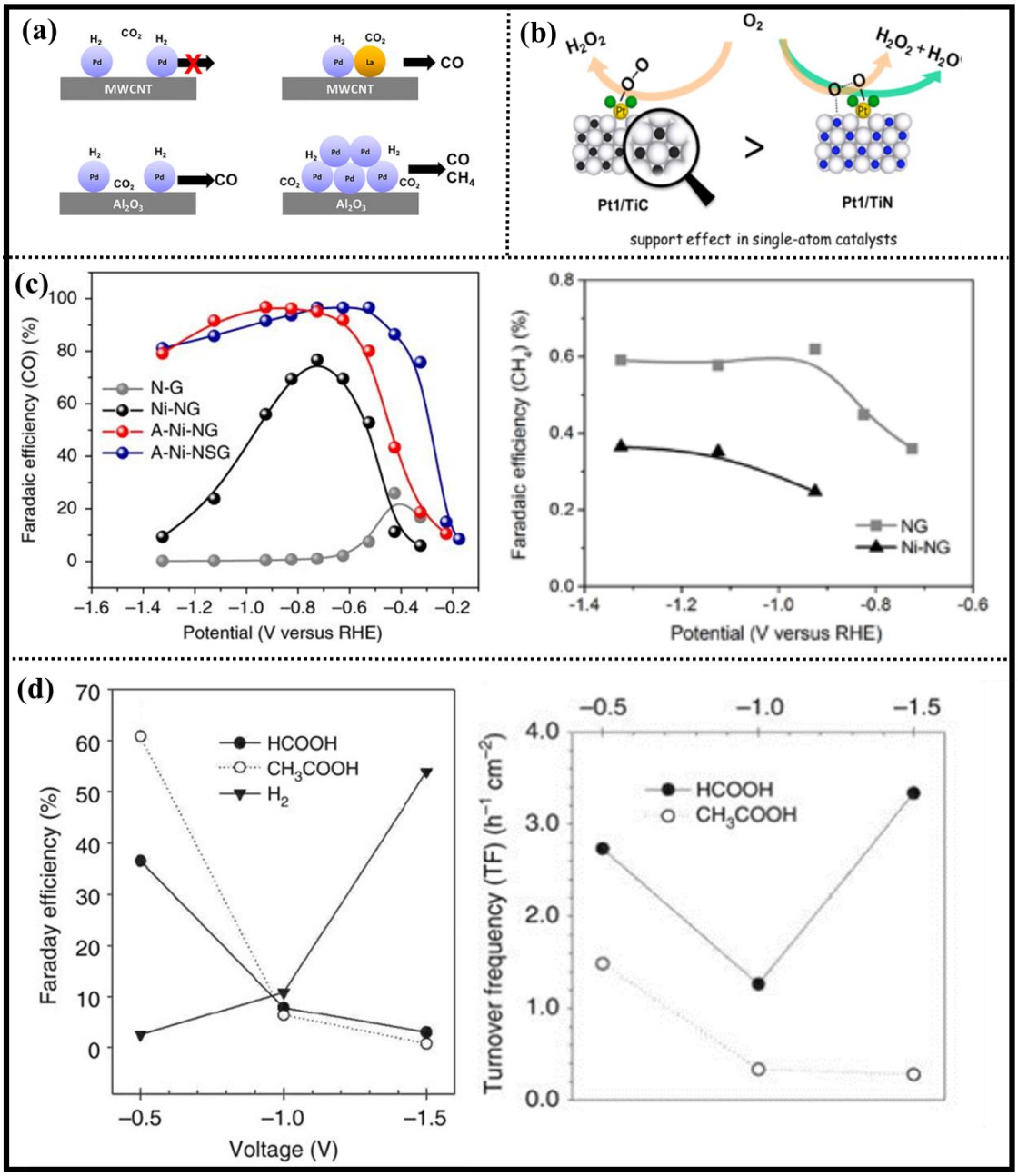

Figure 17. (a) Schematic illustration of the reduction of CO_2 with H_2 on Pd/Al_2O_3 and Pd/MWCNT catalysts. Reproduced with permission. [74] Copyright 2013, American Chemical Society. (b) Support effects for selectivity of ORR reaction with Pt_1 catalysts. Reproduced with permission.[18b] Copyright 2016, American Chemical Society. (c) CO Faradaic efficiency at various applied potentials with different catalysts for CO_2 reduction in aqueous solution. Reproduced with permission.[117d] Copyright 2018, Nature Publishing Group. (d) Faraday

efficiency (%) to the products of CO_2 reduction under applied voltage of -0.5, -1, and -1.5 V vs Ag/AgCl (3M KCl) for Fe_1-N-C sample and corresponding turnover frequency (h^{-1} cm^{-2}). Reproduced with permission.[118] Copyright 2018, Nature Publishing Group.

Heterogeneous single-atom catalysts (SACs) hold a great promise for maximizing atomic efficiency of supported metals by achieving the ultimate utilization of every single atom. The foreign isolated substitutions anchored on different supports build varieties of local structural centres, changing the physical orbital science, band gap, electronic density, and surface chemistry. Thus, distinct atomic local environments for single-atom catalysts are essential on determining superior catalytic performance for a wide variety of chemical reactions. A comprehensive report is summarized from the perspectives of support effects for stable synthesis and high catalytic properties of various SACs. We believe that tuning the interaction by selection of the supports towards favourable atomic and electronic structures on the surface should be taken into account for the development of more efficient SACs.

Keywords: single atom catalysts; support effects; SACs synthesis; catalytic reactions; atomic-local environments

Wei-Hong Lai, Yun-Xiao Wang, Jia-Zhao Wang*, Shu-Lei Chou**

Atomic-local environments of single-atom catalysts: synthesis, electronic structure, and activity

TOC figure